HHS Public Access

Author manuscript

Nat Microbiol. Author manuscript; available in PMC 2020 February 05.

Published in final edited form as:

Nat Microbiol. 2019 December ; 4(12): 2369–2382. doi:10.1038/s41564-019-0518-2.

An RNA-Centric Dissection of Host Complexes Controlling Flavivirus Infection

Yaw Shin Ooi[1,*], **Karim Majzoub**[1,2,*], **Ryan A. Flynn**[3,*,¶], **Miguel A. Mata**[1], **Jonathan Diep**[1], **Jason Kenichi Li**[4], **Nicholas van Buuren**[4], **Neil Rumachik**[3], **Alex G. Johnson**[5], **Andreas S. Puschnik**[1], **Caleb D. Marceau**[1], **Luwanika Mlera**[6], **Jeffrey M. Grabowski**[6], **Karla Kirkegaard**[4], **Marshall E. Bloom**[6], **Peter Sarnow**[1], **Carolyn R. Bertozzi**[3,7], **Jan E. Carette**[1,8,¶]

[1]Department of Microbiology and Immunology, Stanford University, Stanford, CA 94305, USA

[2]INSERM U1110, Institute of Viral and Liver Diseases, University of Strasbourg, 67000, France

[3]Department of Chemistry, Stanford University, Stanford, CA 94305, USA

[4]Department of Genetics, Stanford University, Stanford, CA 94305, USA

[5]Department of Chemical and Systems Biology, Stanford University, Stanford, CA 94305, USA

[6]Biology of Vector-Borne Viruses Section, Rocky Mountain Laboratories, NIAID/NIH, Hamilton, MT 59840, USA

[7]Howard Hughes Medical Institute, Stanford University, Stanford, CA, 94305

[8]Lead contact

Abstract

Flaviviruses including dengue virus (DENV) and Zika virus (ZIKV) cause significant human disease. Co-opting cellular factors for viral translation and viral genome replication at the endoplasmic reticulum (ER) is a shared replication strategy, despite different clinical outcomes. While the protein products of these viruses have been studied in depth, how the RNA genomes operate inside human cells is poorly understood. Using comprehensive identification of RNA binding proteins by mass spectrometry (ChIRP-MS), we took an RNA-centric viewpoint of flaviviral infection and identified several hundred proteins associated with both DENV and ZIKV

[¶]Correspondence to: raflynn@stanford.edu, carette@stanford.edu.

[*]These authors contributed equally to this work

Authors Contributions

Y.S.O., K.M., and R.A.F. were responsible for design and execution of experiments, data analysis, and manuscript preparation. M.A.M. and P.S. performed and analyzed northern blotting assays. J.D. carried out MAGECK analysis for all CRISPR screens results. J.K.L. and N.R. assisted proteomic experiments. N.V.B. and K.K. were responsible for immunofluorescence and FISH assays. A.G.J. assisted preparation of manuscript. A.S.P. and C.D.B. helped preparation of reagents, cell lines, and viruses. L.M., J.M.G., and M.E.B. were responsible for infection assays and analyses involved POWV. J.E.C. and C.R.B, supervised the research, acquired funding, interpreted data and prepared the manuscript.

Data availability

Raw and processed sequencing data can be found at:
https://www.ncbi.nlm.nih.gov/geo/query/acc.cgi?acc=GSE109194

Competing interests

The authors declare no competing financial interests.

genomic RNA in human cells. Genome-scale knockout screens assigned putative functional relevance to the RNA-protein interactions observed by ChIRP-MS. The ER-localized RNA binding proteins vigilin and RRBP1 directly bound viral RNA and each acted at distinct stages in the life cycle of flaviviruses. Thus, this versatile strategy can elucidate features of human biology that control pathogenesis of clinically relevant viruses.

Main

Mosquito-borne flaviviruses such as DENV and ZIKV severely impact global health with an estimated 100 million individuals suffering from DENV-induced illness alone[1,2]. Gaining insights into the mechanisms by which flaviviruses exploit their host environment to promote viral propagation could yield targets for host-directed therapies to combat infections[3,4]. Flaviviruses enter cells via receptor-mediated endocytosis and upon membrane fusion viral genomes are released into the cytoplasm. The ~11 kilobase (kb) flavivirus genomic RNA encodes a single viral polyprotein, which is subsequently cleaved into mature structural and non-structural proteins (NSPs). Biogenesis of the flaviviral proteins, which occurs at ER membranes, is not trivial due to the size of the polyprotein (~3,300 amino acids), the occurrence of multiple transmembrane regions, and the co-translational cleavage by viral and cellular proteases. After an initial round of translation, the RNA serves as a template for RNA replication, which occurs in close association to the ER-membrane and primarily requires the NS5 RNA-dependent polymerase and NS3 helicase with involvement of other NSPs and poorly defined host factors. Viral RNA-protein interactions are essential to recruit and retain the RNA to these ER sites and to mobilize cellular factors required for translation, replication, and packaging[5–7]. Although the viral RNA (vRNA) constitutes a central molecular hub during flavivirus infection, precise molecular details have yet to be unraveled[8]. A global survey of cellular RNA-binding proteins (RBPs) interacting with vRNAs during infection would provide molecular insights into the composition and function of the ribonucleoprotein machines that drive vRNA translation and replication.

Results

Unbiased discovery of the flaviviral genomic RNA protein interactome

To define the compendium of host proteins that associate with the positive-strand viral RNA, we implemented Comprehensive Identification of RNA-binding Proteins by Mass Spectrometry (ChIRP-MS)[9]. The human hepatoma cell line Huh7.5.1, which supports high levels of flaviviral replication, was infected with either DENV-2 or ZIKV at a multiplicity of infection (MOI) of 0.1 for 48 hours. Infected cells were subsequently crosslinked with formaldehyde to preserve *in cell* interactions between proteins and RNAs and stabilize ribonucleoprotein (RNP) complexes. Biotinylated oligonucleotides (Supplementary Table 1) were used to specifically enrich for DENV or ZIKV RNA and recovered proteins were subjected to label-free quantitative LC-MS/MS (Fig. 1a). We recovered roughly 50% of the vRNA across the full length of each vRNA, suggesting robust sampling of the total cellular viral RNAs, while strongly depleting for highly abundant host RNAs such as 7SK and ribosomal RNA as shown by qRT-PCR analysis (Supplementary Fig. 1a). The tiled probes were also able to capture full length DENV-2 RNA from total RNA of infected Huh7.5.1

cells while visibly depleting all other cellular RNAs (Supplementary Fig. 1b and 1c). Together, these experiments provide strong evidence that ChIRP enrichment for DENV and ZIKV RNA is specific and efficient.

Interrogating the ChIRP-MS revealed extensive coverage of both DENV and ZIKV polyproteins including the structural (C, PrM, and E) and non-structural (NS1-NS5) viral proteins (Fig. 1b–d). Analysis of the peptide coverage per protein length, revealed that the viral NS3 and NS5 proteins were most strongly recovered (Supplementary Fig. 1d) consistent with these being RBPs directly binding the flaviviral RNA. Our results are thus in line with ChIRP-MS enriching most strongly for RBPs, but also proteins present in functionally relevant RNA-protein complexes that do not directly interact with the RNA[10].

Beyond the virally encoded polyprotein we identified 464 high confidence hits from the human proteome that were specifically and reproducibly associated with the DENV or ZIKV vRNA (FDR < 0.01, SAINT score >0.99 and enrichment >2 fold over the NI ChIRP-MS, Fig. 1e, Supplementary Table 2, and Methods). The ChIRP-MS was highly consistent across the biological triplicates, confirming strong intra-probe set reproducibility (Supplementary Fig. 1e and 1f). The enrichment of specific host factors recovered with DENV or ZIKV RNA were positively correlated (Pearson's $r = 0.67$ Fig. 1e). Among the highest scoring candidates were RBPs previously implicated in the antiviral response against dengue infection including MOV10[11], YBX1[12], and ADAR[13] as well as proteins with pro-viral functions including SND1[14]. Gene Ontology (GO) annotation revealed the strongest enrichment for the membrane component of cells (Fig. 1f). Protein domain analysis of the hits was enriched for RNA binding domains and the majority of the hits (~75%) overlapped with a comprehensive list of mammalian RBPs[15] (Fig. 1g and Supplementary Table 2). Given the role of the ER membrane in flaviviral translation and the GO enrichment, we examined ER-localized proteins in the ChIRP-MS data. ER-localized proteins were enriched with high statistical significance ($p<0.0001$; Fischer exact test) in the ChIRP-MS dataset (3¼64) when compared to the fraction of ER-localized proteins expressed in Huh7.5.1 cells (421/18199, Methods and Supplementary Table 3 and 4). These data reinforce the notion that ChIRP-MS retrieves RBPs that associate with flaviviral RNA, and that several of these are ER-proteins.

To determine the specificity of the RBPs for flaviviruses, we performed ChIRP-MS on an unrelated single stranded RNA virus from the picornavirus family (rhinovirus, strain RV-B14). We recovered 350 host proteins associated with rhinovirus RNA (Supplementary Table 5). Comparing host proteins associated with DENV or ZIKV with RV-B14 vRNA resulted in a weaker pairwise correlation (Supplementary Fig. 2a and 2b, Pearson's $r = 0.40$ and 0.13 respectively) than between the two flaviviruses. Further, RV did not statistically enrich for ER-annotated factors (5/350 hits, Supplementary Fig. 2c and Supplementary Table 3), underscoring the important role the ER membrane plays in flaviviral biology. Thus, the DENV and ZIKV ChIRP-MS experiments provide a valuable resource of host-factors that associate with flaviviral positive strand RNA.

Genome-wide knockout screens reveal functional ChIRP-MS host factors

We and others have previously reported genome-wide knockout (KO) screens for DENV-2 (type strain 16681), ZIKV (African type strain MR766), and West Nile virus[16–19]. Here we provide a higher granularity view to these studies by interrogating multiple serotypes and clinical isolates. We performed four CRISPR/Cas9 screen in Huh7.5.1 cells by infecting them with four recently isolated and low-passaged DENV serotypes (i.e. 1, 2, 3, and 4). For ZIKV, we performed haploid genetic screens utilizing three ZIKV strains isolated during recent epidemics in French Polynesia (FP/13), Puerto Rico (PRVABC59), and Colombia (FLR). The screen results were consistent and reproducible across DENV serotypes and ZIKV strains (Supplementary Table 6). We merged the enrichment scores of the respective DENV (Fig. 2a) and ZIKV (Supplementary Fig. 3a) screens to obtain core sets of genes critical for flavivirus infection. Most of the identified host factors and pathways were related to biogenesis of ER-targeted proteins and were common between DENV and ZIKV (Supplementary Fig. 3b and 3c, Supplementary Table 6). Collectively, these data represent a saturating analysis of host factors through seven genome-wide KO screens and highlight the importance of specific intracellular ER-associated protein complexes for DENV and ZIKV infection.

Because the DENV forward genetic screens and the ChIRP-MS were performed in the same Huh7.5.1 cell line, we compared these orthogonal techniques. Intersection of the top 200 hits from the DENV KO screens with the ChIRP-MS resulted in 10 co-occurring proteins (Fig. 2b and Supplementary Table 6). Several subunits of the OST complex (STT3A, STT3B, RPN2, and MAGT1) are top hits in this data set, both associating with the vRNA and of central importance for viral replication[16] (Fig. 2b). ASCC3 and SND1 were previously described to be important as regulators of the cellular transcriptional response to flavivirus infection or as directly binding to vRNA, respectively[14,20]. Finally, two factors (vigilin and RRBP1), which have not been previously linked to flavivirus infection, stood out as among the most enriched in the ChIRP-MS (Supplementary Table 2 and Fig. 2b). We therefore focused on characterizing the molecular properties of these RBPs, as well as defining the stages of the flaviviral life cycle at which these RBPs act.

To assess the impact of RRBP1 and vigilin on flaviviral infections we generated isogenic knockout lines (RRBP1-KO and vigilin-KO) in Huh7.5.1 cells (Fig. 2c). We then challenged RRBP1-KO and vigilin-KO cells with DENV, ZIKV, and Powassan virus (POWV) all belonging to the flavivirus genus, or Chikungunya virus (CHIKV), an alphavirus. Viral RNA loads were significantly reduced in the knockout cells for most of the tested flaviviruses, but CHIKV RNA levels were unaffected (Fig. 2d and 2e). The reduction of ZIKV infectivity in the knockout cells was further validated using a luciferase-expressing ZIKV (ZIKV-Luc) (Supplementary Figure 3d). Thus, RRBP1 and vigilin are broadly required for members of the mosquito-borne (DENV, ZIKV) and tick-borne (POWV) flaviviruses but not for the unrelated arbovirus CHIKV. The abundance of viral proteins (e.g. prM and NS3) was noticeably decreased in RRBP1-KO and vigilin-KO cells (Fig. 2f). The absence of RRBP1 and vigilin also led to significant decrease in production of infectious progeny virions (Fig. 2g). These results solidified RRBP1 and vigilin as host factors that promote flavivirus infections.

RRBP1 and vigilin interact at the ER

Ribosome-binding protein 1 (RRBP1/p180) is a highly-expressed RBP anchored to the ER via a N-terminal transmembrane domain, which can act as an mRNA receptor at the ER[21]. Vigilin promotes translation of a subset secretory mRNAs at the ER but in contrast to RRBP1, lacks a transmembrane domain to anchor it to the ER[22]. Confocal microscopy revealed that both RRBP1 and vigilin co-localized with ER-GFP, a previously reported ER marker[23], with RRBP1 exhibiting a slightly higher correlation than vigilin (Fig. 3a and Supplementary Fig. 4a, 0.69 and 0.60, respectively). To more directly assess association with ER membranes, we used a subcellular fractionation assay, which relies on a mild digitonin lysis to separate ER membranes from cytosolic contents[24]. RRBP1 exclusively co-fractionated with the ER fraction whereas vigilin was found in both ER and cytosolic fractions (Fig. 3b). To test whether RRBP1 and vigilin associate with each other, we performed co-immunoprecipitation (co-IP) experiments. We found that vigilin co-IPed with RRBP1 in non-infected and DENV infected cells (Fig. 3c and Supplementary Fig. 4b). RNase A treatment reduced the co-recovery of vigilin with RRBP1 markedly, suggesting that this interaction was RNA dependent (Fig. 3c and Supplementary Fig. 4b). Finally, during infection with DENV and ZIKV, both proteins co-localized with positive-stranded vRNA (Fig. 3d, 3e, Supplementary Fig. 4c, and 4d). Taken together, our data indicate that RRBP1 and vigilin interact in an RNA-dependent manner at the ER near to the positive-stranded viral RNA.

Global characterization of RNAs associated with RRBP1 and vigilin

To examine the interaction of RRBP1 and vigilin with viral and cellular RNA during infection we performed infrared crosslinking and immunoprecipitation (irCLIP)[25] on non-infected and virus-infected cells. Primary antibodies targeting RRBP1 and vigilin generated irCLIP RNAse-sensitive signal that was specific to their respective RBPs (Supplementary Fig. 5a and 5b). Further, analyzing proteins co-enriched with RRBP1 or vigilin irCLIP enrichments near their molecular weight via MS confirmed their specificity (Supplementary Fig. 5c and 5d). Sequencing the enriched RNAs revealed a preference for ribosomal RNA (66% rRNA) over messenger/noncoding RNA (33% mRNA/ncRNA) binding for RRBP1 (Fig. 4a), in line with its known direct association with ribosomes[26]. RRBP1 crosslinks to many sites across rRNAs with a strong peak in the 18S rRNA on helix 18 (H18) positioned near the mRNA entry channel[27] (Fig. 4b[27]). In contrast to RRBP1, vigilin reverse transcriptase (RT) stops mainly mapped to mRNA/ncRNAs with only minor contribution of rRNA (Fig. 4a). Interestingly, while vigilin has more restricted rRNA binding pattern, its major binding site is on H16 of the 18S rRNA, adjacent to the RRBP1 bound position at the mRNA entry channel (Fig. 4b).

Infection with DENV or ZIKV resulted in the appearance of reads derived from the viral positive stranded genome for both RRBP1 and vigilin. The change in binding profile was especially apparent for vigilin, where 75% or 49% of all crosslinks mapped to the vRNA, respectively (Fig. 4a). Globally, for both RRBP1 and vigilin, RT stops mapping the mRNAs were depleted in intronic regions suggesting a preference for mature transcripts (Fig. 4c). Vigilin preferentially bound exonic regions whereas RRBP1 binding was enriched for binding to exons as well as 5’ and 3’ UTRs (Fig. 4c). For both RRBP1 and vigilin, GO

analysis of the bound mRNAs revealed terms related to membrane-bound and secreted proteins known to be highly expressed in hepatic cells (Supplementary Table 7 and 8)[28,29]. For RRBP1, in the context of infection, there was weaker enrichment for membrane terms, while there was a gain of novel terms such as cytosol and ribosome, suggesting differential localization of these mRNAs upon infection (Supplementary Fig. 5e). For vigilin, the enrichments were quite similar between infected and non-infected cells (Supplementary Fig. 5f).

Next, we visualized the RT stops mapping to DENV or ZIKV RNA. RRBP1 crosslinked across the full-length positive strand vRNA with RT stops extending into the 5' and 3'UTRs (Fig. 4d and Supplementary Fig. 6a). In contrast, vigilin bound to the coding region but markedly less RT stops were observed in the 5' and 3'UTRs (Fig. 4d). This pattern was similar to what was observed with cellular mRNAs (Fig. 4c, Supplementary Fig. 6b, and 6c) and is in line with previously reported preference for binding to coding regions[22]. For both RBPs, we observed rather uniform binding throughout the vRNA without apparent hotspots. On a per nucleotide basis, RRBP1 and vigilin binding was positively correlated on the DENV and ZIKV genomes (r = 0.79 and 0.84, respectively, Supplementary Table 7 and 8), but were not correlated to cDNA truncations from RNA-seq of the viral vRNA suggesting the irCLIP profiles are specific (Supplementary Table 7 and 8). This broad 'coating' of the vRNA is reminiscent of how other RBPs such as FMRP bind actively translating mRNAs[30]. Together, the comparative RNA binding profiles of RRBP1 and vigilin show that both proteins engage cellular rRNA and secretory mRNAs with RRBP1 having a higher proportion of rRNA binding. During infection, both RBPs bind flavivirus RNA and for vigilin the majority of RT-stops retrieved are of flaviviral origin.

RRBP1 and vigilin are required for optimal translation and replication of DENV

We further defined the step(s) at which the RBPs act in the viral life cycle by utilizing a luciferase-expressing DENV (DENV-Luc). First, we generated additional RRBP1 and vigilin clonal knockout cell lines in HEK293 cells to mitigate potential cell-type specific effects (Supplementary Fig. 7a and 7b). RRBP1 and vigilin deficiency resulted in decreased luciferase expression throughout the infection cycle for DENV-Luc but not for the unrelated Coxsackievirus B3 virus expressing luciferase (Fig. 5a–d). Re-expression of RRBP1 and vigilin rescued, at least partially, the defect in flavivirus translation and replication indicating that it is specific for the knockout. To separate the translation and replication phase of the viral life cycle from the viral entry and uncoating steps, we transfected *in vitro* transcribed DENV replicon in which the structural proteins are replaced with the *Renilla* luciferase gene. Compared to wild type (WT) cells, knockout of both RBPs resulted in decreased luciferase expression throughout the time course (Fig. 5e and 5f). Because viral entry is bypassed in this experiment, these results suggest that RRBP1 and vigilin promote optimal viral translation and replication rather than viral entry.

Viral translation and replication are intricately linked: after initial translation, viral NSPs are produced that replicate genomic RNA, which in turn produces more mRNA templates resulting in increased translation. Early in infection, a greater contribution of initial translation is expected, whereas in later time points, it is a combination of viral translation

and replication. To examine this in more detail and to assess RRBP1 and vigilin's respective contributions to these phases, we performed DENV-Luc infections in the presence or absence of the DENV RNA replication inhibitor MK0608[31]. Control experiments confirmed that the luciferase signal at 8 hours post infection (hpi) in the presence of MK0608 represents initial viral translation whereas at 36 hpi (in the absence of MK0608) the bulk of the signal is due to subsequent RNA replication and translation (Supplementary Fig. 7c and 7d). Compared to WT, RRBP1 deficiency resulted in an approximately 2-fold reduction of luciferase expression at 8hpi whereas vigilin deficiency did not decrease luciferase expression (Fig. 5g). However, at 36 hpi vigilin-KO showed a more severe phenotype than RRBP1-KO (7× vs. 3× reduction, respectively). We therefore conclude that the role of RRBP1 is more pronounced during the early stage of infection whereas vigilin plays a more significant role at later stages of infection.

Cellular RBPs contribute to DENV genomic RNA stability

To further characterize the role of RRBP1 and vigilin, we generated an isogenic cell line that is deficient in both RRBP1 and vigilin in Huh7.5.1 cells (Fig. 6a). We observed a stronger decrease in the single RRBP1-KO cells compared to vigilin-KO early in infection and the reverse pattern later in infection with DENV-Luc, corroborating the RBP-KO viral phenotypes in HEK293 cells (Fig. 5g). The RRBP1-vigilin double knockout cells displayed an early defect comparable to the RRBP1-KO cells and a late defect that was stronger than the vigilin-KO (Fig. 6b) suggesting that both RBPs are required for optimal replication.

Our results combined with the known role of RRBP1 and vigilin in translation of cellular mRNAs[32,33] suggests that the RBPs stimulate viral RNA replication, at least partially, by promoting translation of the viral polyprotein. Aside from translation, both vigilin and RRBP1 can also act on the stability of their target mRNAs[34,35]. To assay for viral vRNA accumulation, we used MK0608 to inhibit viral replication and northern blotted against the DENV 3'-UTR, allowing detection of vRNA decay (Fig. 6c). We observed that the accumulated DENV genomic RNA was relatively stable in the WT cells, up to 24 hours post MK0608 treatment (Fig. 6c, Supplementary Fig. 8a). In contrast, in the absence of both RRBP1 and vigilin the decay rate of the gRNA was accelerated (Fig. 6c and Supplementary 8b). Taken together, our data indicate that RRBP1 and vigilin promote optimal flavivirus infection and have roles in viral RNA translation, replication, and stability.

Discussion

Our results provide detailed insights into the molecular identity of the host machineries engaged by flaviviral RNA during infection. We have comprehensively mapped the interactions between the flaviviral RNA genome and the human cellular proteome during viral infection using ChIRP-MS. Intersecting this dataset with a core set of genes identified in our genetic screens using all serotypes of DENV and multiple strains of ZIKV (Supplementary Table 9) highlighted the importance of ER-localized RBPs for flavivirus infection. One example of an ER-localized RBP was RRBP1 which has a short luminal domain, a transmembrane domain, and a large domain facing the cytosol that is highly basic and contains a decapeptide tandem repeat motif[36]. RRBP1 can act as a minor polysome

receptor at the ER membrane[37], while it can also bind certain mRNAs in a ribosome-independent fashion[33]. Our data support these non-mutually exclusive views of RRBP1 function: the majority of RT stops identified from RRBP1 irCLIP are indeed from the rRNA but nearly one-third of binding maps to mRNAs enriched for secretory protein transcripts (e.g. APOB and AFP).

Vigilin is an evolutionarily conserved RNA-binding protein that interacts with RNA through its KH domains. While vigilin has been reported to be predominantly cytosolic, associating with free ribosomes[38], we detect a portion of vigilin in the ER fraction, corroborating previous observations of its association ribosomes at the rough ER[39,40]. We found that vigilin directly binds to rRNA and is preferentially enriched for binding to a subset of cellular mRNAs that encode secretory proteins, indicating a potential role in translation. This is consistent with the emerging view of vigilin as a translational enhancer for a subset of mRNAs of the secretory pathway[22,41]. Our results indicate that DENV and ZIKV co-opt vigilin to promote infection.

Determining the protein interactome of RNA viruses has been a long-standing question of the field and is of interest to many laboratories. Two recent reports that utilized UV-crosslinking and dengue RNA pulldown[42,43] found 12 and 93 host RBPs, respectively, which partially overlaps with our ChIRP-MS data (Supplementary Table 10). We used ChIRP-MS as a robust platform to discover the protein interactomes of vRNA. We were careful to verify that the enrichment procedure would recover proteins binding across the entire length of the 11kb viral genome as well as sample a majority of the vRNA from infected cells. These quality controls ensured the resulting proteomic data would be as robust and complete as possible. Further, as a discovery tool, we opted for chemical crosslinking, which provides the context of RBP complexes associated with the target RNA.

Our study of the flavivirus RNA-interactome is a valuable resource that provides an RNA-centric perspective on viral infection, complementing other large-scale approaches that map virus-host interactions. The strategy employed here, integrating RNA-protein interactome data with genome-scale knockout screening, is a generalizable strategy for the study of the complex interactions of cellular proteins with other RNA viruses. Critically, rigorous validation through isogenic knockouts of host factors and direct but unbiased assessment of their RNA interactomes with irCLIP, provides a robust platform for discovery of functional interactions. The approach emphasizes the RBPs that have a pro-viral role because of the design of the genetic screens, but can readily be modified to include other large-scale approaches that identify proteins with antiviral activities[44].

Methods

Cell lines, reagents and generation of knock-out cells

HAP1 cells were derived from the near-haploid chronic myeloid leukemia cell line KBM7[45]. HAP1 cells were cultured in IMDM supplemented with 10% heat-inactivated fetal bovine serum (HI-FBS), penicillin-streptomycin and L-glutamine. BHK-21 (ATCC), HEK293FT (Thermo Fischer Scientific), H1-HeLa cells (ATCC), Huh7.5.1 (generous gifts from Frank Chisari), RD (ATCC), BHK-21 (ATCC), and Vero (ATCC) cells and knock-out derivatives

were cultured in DMEM media supplemented with 10% HI-FBS, 1× penicillin-streptomycin and 1× L-glutamine. C6/36 cells (ATCC) were purchased from ATCC and were cultured in Leibovitz's L-15 Medium supplemented with penicillin-streptomycin, L-glutamine, and 10% HI-FBS. Cycloheximide was purchased from Sigma-Aldrich. MK0608 (7-Deaza-2'-C-methyladenosine) was purchased from Carbosynth (San Diego, CA).

To generate RRBP1 and vigilin knock-out cell lines CRISPR-Cas9 strategy was employed. CRISPR guide RNA sequences were designed using the Zhang lab CRISPR design tool (http://crispr.mit.edu) and corresponding oligos were purchased from Integrated DNA Technologies. Oligos were cloned into the Zhang lab generated Cas9 expressing pX458 guide RNA plasmid (Addgene #48138) as previously described[16]. The cloning products were transfected into HEK293FT and Huh7.5.1 cells using Lipofectamine 3000 (Thermo Fisher Scientific) and were subsequently single-cell sorted based on GFP into 96-well plates using a BD Influx cell sorter at the Stanford Shared FACS facility. Clonal cell lines were allowed to expand from a single cell and genomic DNA was isolated for sequencing-based genotyping of targeted alleles. For this, a 300–500 base-pair (bp) region that encompassed the guide RNA-targeted site was amplified and the sequence of the PCR product was determined by Sanger sequencing. Subclones were chosen where all alleles were mutated with insertions or deletions that weren't a factor of 3. Knock-out subclones verified by genotyping were further confirmed by Western blot using antibodies against RRBP1 (Bethyl Laboratories, A303–996A) or Vigilin (Bethyl Laboratories, A303–971A). Guide RNA primers are listed in Supplementary Table 1 and cloned into the PX458 plasmid. RRBP1/Vigilin double knock-out Huh7.5.1 cell lines were generated by transfecting verified RRBP1-KO cells with the same PX458 plasmid containing vigilin guide RNA used earlier to knock-out vigilin. Double knockout selection and characterization was performed by western blot analysis on single-cell FACS sorted clonal cells.

Viral strains, serotypes, reporter viruses, and replicon

DENV-2 infectious clone 16681 was a generous gift from Dr. Karla Kirkegaard, Stanford University. DENV-2 derived from infectious clone 16681 was a cell culture (HAP1 cells) adapted strain[16]. DENV-1^{276RKI} (#NR-3782, isolated in 1997 from a human in India), DENV-2^{429557} (#NR-12216, isolated in 2005 in Mexico), DENV-$3^{Philippines/H871856}$ (#NR-80, isolated in 1956 from human serum in the Philippines), DENV-$3^{VN/BID-V1009/2006}$ (NR-44088, isolated in 2006 from a human in Vietnam) and DENV-$4^{BC287/97}$ (#NR-3806, isolated in 1997 from a human in Mexico), $ZIKV^{FLR}$ (Human/2015/Colombia, NR-50183) and $ZIKV^{PRVABC59}$ (Human/2015/Puerto Rico; NR-50240) were obtained from BEI resources (NIH, NIAID). $ZIKV^{H/PF/13}$ French Polynesia was provided by Dr. Catherine Blish, Stanford University. All DENV serotypes and ZIKV isolates were propagated in C6/36 cells. Production of DENV and ZIKV infectious particles were always tittered by standard plaque assays on Huh7.5.1 cells, unless otherwise stated. Chikungunya virus (CHIKV 18½5 vaccine strain) was a generous gift from Dr. Margaret Kielian and was propagated and titered by standard plaque assay in BHK-21 cells. Powassan virus (POWV) LB prototype strain (originally obtained from Robert Tesh, University of Texas Medical Branch)[46] stock was amplified and titered by standard plaque assay in Vero cells.

Luciferase-encoding ZIKV infectious clone (ZIKV-Rluc) was kindly provided by Dr. Pei-Yong Shi, UTMB, Galveston, Texas and the viral stock was generated in Vero cells as described[47]. Coxsackievirus B3 Nancy strain that encodes Renilla luciferase (CVB3-Luc) was a generous gift from Dr. Frank van Kuppeveld, and propagated by transfection of the infectious clone pRLuc-53CB3/T7 into RD cells[48]. The titer of CVB3-Luc was determined by standard plaque assay on H1-HeLa cells.

Construction of pDENV-Luc infectious clone was performed as described[16]. The viral 5'UTR was followed by a duplication of the first 104 nucleotides of the C coding region, which contain cis-acting elements required for replication (CAE). The CAE was fused to the Renilla luciferase coding region followed by the complete DENV open reading frame (ORF). Between the luciferase and the DENV structural proteins a foot and mouth disease virus (FMDV) 2A sequence was introduced to provide co-translational cleavage and release of luciferase. The construct was based on pD2/IC-30P, which contains a full-length infectious clone encoding DENV-2^{16681} in which an envelope protein (E) Q399H mutation was introduced that enhanced viral infection in mammalian cells using primers (Supplementary Table 1) via the QuikChange Site-Directed Mutagenesis kit (Agilent Technologies, Santa Clara, CA). We gene-synthesized a fragment containing the T7 polymerase promoter sequence followed by the first 104 nucleotides of the C coding region in frame with Renilla luciferase and FMDV 2A. This fragment was PCR amplified, introducing a SacI site at the 5' end and a NheI site (present in the FMDV 2A sequence) at the 3' end using primers (Supplementary Table 1). To create and in frame fusion of FMDV 2A with the DENV-ORF a second DNA fragment was amplified using pD2/IC-30P as template with primers (Supplementary Table 1) to introduce 5' NheI and 3' SphI restriction sites. The two fragments were cut with the respective restriction enzymes and ligated into pD2/IC-30P cut with SacI and SphI to create pDENV-Luc. DENV-Luc virus was produced by cutting with XbaI to linearize plasmid and *in vitro* transcription performed of pDENV-Luc using the MEGAscript T7 transcription kit (AM1334) and transfection into BHK-21 cells using lipofectamine 2000. Filtered supernatant of transfected BHK-21 cells was used to infect Huh7.5.1 cells.

Construction of the DENV WT replicon was described previously[16]. As per the pDENV-Luc except that the Renilla luciferase coding region was directly followed by the DENV ORF starting at the signal peptide preceding NS1, deleting the structural proteins. The construct was based on pD2/IC-30P, which contains a full-length infectious clone encoding DENV-2^{16681}. We gene-synthesized a fragment containing the T7 polymerase promoter sequence followed by the first 102 nucleotides of the C coding region in frame with Renilla luciferase and FMDV 2A followed by the DENV open reading frame (ORF) starting at the signal peptide preceding NS1 until an internal HpaI site. This fragment was released by SacI (preceding the T7 promoter) and HpaI and cloned in pD2/IC-30P in a three-point ligation with KpnI/SacI and KpnI/HpaI fragments. Primer sequences are listed in Supplementary Table 1.

Constructs and packaging of lentivirus

To generate a lentiviral construct expressing GFP-RRBP1 cDNA construct was generously provided by Alex Palazzo, University of Toronto[21] and was used as template to generate a PCR product using primers listed in Supplementary Table 1. Amplified PCR product was then cloned with the Gibson assembly reaction kit (New England Biolabs, UK) into pLenti-CMV-Puro-Dest (w118–1) that was EcoRV digested. Vigilin cDNA (a.k.a. HDLBP; MGC cDNA BC001179) were purchased from GE Dharmacon. The cDNA was amplified in two separate fragments using primers listed in Supplementary Table 1. Both PCR fragments were cloned by Gibson Assembly (New England Biolabs) into the EcoRV digested third generation lentiviral Gateway destination vector, pLenti-CMV-Puro-Dest(w118–1), that drives transgene expression by a CMV promoter and harbors puromycin resistant gene as a selectable marker.

The ER marker, ER-GFP, was engineered according to a previously reported construct[23]. EGFP fused with an N-terminal signal peptide of calreticulin and a C-terminal KDEL ER retention sequence was synthesized in two fragments (Integrated DNA Technologies) and cloned by Gibson Assembly (New England Biolabs) into pLenti-CMV-Puro-Dest(w118–1) expression vector.

Lentiviral or retroviral transduction was used to create stable cell lines expressing a selected gene of interest. Respective genes of interest were cloned into the pLenti-CMV-Puro-DEST vector (w118–1) (a gift from Eric Campeau). Lentivirus was propagated by co-transfection of the transgene expressing plasmid with a mixture of ΔVPR, VSV-G, and pAdVAntage packaging plasmids into HEK293FT cells using FuGENE HD (Promega). At 48 hours post-transfection, lentivirus was harvested from the supernatant and filtered through a 0.45-micron filter. 1× protamine sulfate was added to the lentivirus before transducing respective cell lines for overnight. Cells stably expressing the gene of interest were selected by treatment with 1–4 μg/mL puromycin over 2 days (InvivoGen) along with untransduced cells as negative controls. A lentivirus carrying either the mCherry (RFP) gene or the empty pLenti-CMV-Puro-DEST vector was used as a control for RRBP1 and vigilin complementation in the KO cell lines, respectively.

Quantitation of virus infectivity by quantitative RT-PCR (qRT-PCR)

Experiments where viral RNA loads were determined by qPCR were performed as following: 20,000 HEK293FT, Huh7.5.1 cells or their derivatives were seeded in triplicate in 96-well plates one day before infection. The next day, cells were infected with the indicated virus and MOI. At indicated times post-infection, cells were lysed with the lysis buffer from Ambion Power SYBR Green Cell-to-Ct kit (Ambion, 4402954). Reverse Transcription (RT) and qPCR were performed according to the Cell-to-Ct kit instructions on a Bio-Rad CFX Connect quantitative-PCR (qPCR) machine. All Ct values were normalized to the 18S ribosomal RNA expression values. qRT-PCR primers are listed in Supplementary Table 1.

Powassan virus infection, RNA extraction and RT-qPCR analysis

Cells were seeded in triplicate at 1×10^5 cells/well in a 24-well plate and incubated overnight Following overnight incubation, the DMEM was aspirated and the cells were

washed twice with PBS. The cells were then infected with POWV LB strain at a multiplicity of infection of 0.1. At 48 hpi, POWV-infected cells were washed twice with PBS and the cells were lysed in 350 μL of RLT buffer (Qiagen). Total RNA was extracted using an RNeasy mini kit (Qiagen). cDNA was synthesized from 400 ng of total RNA template using the iScript cDNA synthesis kit (BioRad). Primers targeting the positive strand POWV genome (Supplementary Table 1) were used to quantify POWV transcripts as a measure of POWV genome replication relative to the 18s rRNA gene. To determine the efficient annealing temperature for the qPCR analysis, a gradient PCR was conducted using Phusion high-fidelity PCR master mix with HF buffer (NEB). cDNA template prepared from POWV-infected cell RNA, the two primer pairs and the following thermocycler conditions: 94 °C for 5 min; 32 cycles of 94 °C for 15 s, 62–68 °C for 30 s and 72 °C for 2 min; and 72 °C for 7 min. Following gel electrophoresis on E-gel 1.2% agarose with SYBR Safe (Life Technologies), an annealing temperature with amplicons of expected size with no nonspecific amplification was chosen. qPCR reactions were performed on the Applied Biosystems QuantStudio 6 Flex Real-Time system (Life Technologies) in Micro-Amp Optical 384-well reaction plates (Life Technologies). The QuantStudio Real-Time PCR software (v1.3) and the ΔΔCt method were used to calculate the relative POWV transcripts.

Detection of DENV proteins using immunoblotting

Huh7.5.1 WT cells their derivatives were seeded in quadruplet at 1×10^5 cells/well in a 24-well plate and incubated overnight. Cells were then infected with DENV-2 429557 at MOI of 0.1. At 72 hours post-infection, cells were harvested using RIPA buffer (TEKNOVA) supplemented with Laemmli sample buffer (Bio-Rad) and 5% beta-mercaptoethanol (Bio-Rad). Cell lysates were then boiled for 10 minutes and separated by SDS-PAGE on pre-cast 4–15% poly-acrylamide gels (Bio-Rad) in Bio-rad Mini-PROTEAN gel system. Proteins were transferred onto PVDF membranes. PVDF membranes were blocked with PBS buffer containing 0.1% tween-20 and 5% non-fat milk. Blocked membranes were incubated with primary antibody diluted in blocking buffer and incubated overnight on a rocker at 4°C. Primary antibodies were subsequently detected using HRP-conjugated secondary anti-mouse or anti-rabbit antibodies (Genetex) by incubating membranes with 1:5000 dilution for 1 hr at room temperature. Antibody bound proteins were detected by incubating with SuperSignal West Pico PLUS Chemiluminescent Substrate or Dura Extended Duration Substrate (Thermo Fisher Scientific) peroxide solutions and visualized on Bio-Rad ChemiDoc Touch Imaging System. The following primary antibodies were used: anti-prM (Genetex GTX128092) at a dilution of 1:2500; anti-NS3 (Genetex GTX124252) at a dilution of 1:2500; anti-GAPDH (Genetex GTX 627408) at dilution of 1:5000.

Luciferase reporter virus and DENV replicon luciferase assays

For Luciferase reporter virus assays, HEK293FT or Huh7.5.1 cells were seeded in 96-well plates (20,000 cells per well and 10,000 cells per well, respectively) and infected with DENV-Luc or ZIKV-Luc at an MOI of 0.01. The final concentration of the DENV replication inhibitor MK0608 used in this study was always 50 μM. Cells were incubated with the viruses at 37°C with 5% CO_2 and cell lysates were harvested at indicated times. Luciferase expression was measured using Renilla Luciferase Assay system (Promega E2820). Cells were lysed using Renilla lysis buffer and luciferase activity measured by

addition of substrate and immediate luciferase readings were taken using Glomax 20/20 luminometer using a 5 sec integration time.

For Renilla luciferase-expressing DENV replicon assays, the Dengue replicon plasmid was linearized using XbaI restriction enzyme. Replicon RNA was generated using the MEGAscript T7 High Yield Transcription Kit (Ambion AM1334) with the reaction containing 5mM $m^7G(5')ppp(5')G$ RNA Cap Structure Analog (NEB S1405S). Resulting RNA was purified by sodium acetate ethanol precipitation. HEK293FT cells were washed twice with PBS and re-suspended in electroporation buffer (Teknova E0399). 3 μg of purified replicon RNA was mixed with cells and cells were electroporated using Bio-Rad Gene Pulser Xcell electroporator using square wave protocol. Electroporated cells were resuspended in cell culture medium without antibiotics and plated into 96-well plates. Luciferase expression was measured using Renilla Luciferase Assay system (Promega E2820). Cells were lysed at indicated times using Renilla lysis buffer and luciferase activity was measured by addition of substrate and luciferase readings were taken immediately using Glomax 20/20 luminometer using a 5 second integration time.

Infrared Crosslinking and Immunoprecipitation

irCLIP was performed as in [25]. A total number of 7.5 million Huh7.5.1 were seeded and infected next day with DENV-2^{16681} or $ZIKV^{PRVABC59}$ at MOI of 0.1. At 48 hpi, infected cells were UV crosslinked to a total of 0.35 J/cm^2. Whole-cell lysates were generated in CLIP lysis buffer (50 mM HEPES, 200 mM NaCl, 1 mM EDTA, 10% glycerol, 0.1% NP-40, 0.2% Triton X-100, 0.5% N-lauroylsarcosine) and briefly sonicated using a probe-tip Branson sonicator to solubilize chromatin. Each experiment was normalized for total protein amount, typically 1 mg, and partially digested with RNase A (Thermo Fisher Scientific, EN0531) for 10 min at 37°C and quenched on ice. RRBP1 (Bethyl, A303–996A), Vigilin (Bethyl, A303–971A), or IgG (Thermo Fisher Scientific, 02–6102) IP's were performed, 15 μg each antibody with 50 μL Protein A Dynabeads (Thermo Fisher Scientific), for 8 hours at 4°C on rotation. Samples were washed sequentially in 1 mL for 1 min each at 25°C: 1× high stringency buffer (15 mM Tris-HCl, pH 7.5, 5 mM EDTA, 2.5 mM EGTA, 1% Triton X-100, 1% sodium deoxycholate, 120 mM NaCl, 25 mM KCl), 1× high salt buffer (15 mM Tris-HCl pH 7.5, 5 mM EDTA, 2.5 mM EGTA, 1% Triton X-100, 1% sodium deoxycholate, 1 M NaCl), 2× NT2 buffer (50 mM Tris-HCl, pH 7.5, 150 mM NaCl, 1 mM $MgCl_2$, 0.05% NP-40). After the NT2 wash, RNA-protein complexes were dephosphorylated with T4 PNK (NEB) for 45 min in an Eppendorf Thermomixer at 37°C, 15 seconds 1400 rpm, 90 seconds of rest in a 30 μL reaction, pH 6.5, containing 10 units of T4 PNK, 0.1 μL SUPERase-IN (Thermo Fisher Scientific), and 6 μL of PEG-400 (16.7% final). Dephosphorylated RNA-protein complexes were then rinsed once with NT2 buffer and 3'-end ligated with T4 RNA Ligase 1 (NEB) overnight in an Eppendorf Thermomixer at 16°C, 15 seconds 1400 rpm, 90 seconds of rest in a 60 μL reaction containing 10 units T4 RNA Ligase, 1.5 pmol pre-adenylated-IR800–3'biotin DNA-adapter, 0.1 μL SUPERase-IN, and 6 μL of PEG400 (16.7% final). The following day, samples were again rinsed once with 500 μL NT2 buffer and resuspended in 30μL of 20 mM DTT, 1× LDS (Thermo Fisher Scientific) in NT2 buffer. Samples were heated to 75°C for 10 min, and released RNA-protein complexes were

separated on 4–12% Bis-Tris SDS-PAGE (1.0 mm × 12 well) at 200V for 45 min. Resolved RNP complexes were wet-transferred to nitrocellulose at 550 mA for 45 min at 4°C.

Nitrocellulose membranes were imaged using an Odyssey CLx scanner (LiCor), RBP-RNA complexes were excised using scalpels, and RNA was recovered by adding 0.1 mL of Proteinase K reaction buffer (100 mM Tris, pH 7.5, 50 mM NaCl, 1 mM EDTA, 0.2% SDS) and 5 μL of 20mg/mL Proteinase K (Thermo Fisher Scientific). Proteins were digested for 60 min at 50°C in an Eppendorf Thermomixer. Next, 200 μL of saturated-phenol-chloroform, pH, 6.7 was added to each tube and incubated for 10 min at 37°C in an Eppendorf Thermomixer, 1400 rpm. Tubes were briefly centrifuged and the entire contents transferred to a 2 mL Heavy Phase Lock Gel (5Prime, 2302830). Samples were centrifuged for 2 min at >13000 rpm. The aqueous layer was re-extracted with 1 mL of chloroform (inverting 10 times to mix; no vortexing) in the same 2 mL Phase Lock Gel tube and centrifuged for 2 min at >13000 rpm. The aqueous layer was then transferred to a new 2 mL Heavy Phase Lock Gel tube and extracted again with an additional 1 mL of chloroform. After 2 min centrifugation at >13000 rpm, the aqueous layer was transferred to a siliconized 1.5 mL tube and precipitated overnight at −20°C by addition of 10 μL 5M NaCl, 3 μL Linear Polyacrylamide (Thermo Fisher Scientific) and 0.8 mL 100% ethanol. RNA fragments were pelleted at >13000 rpm for 45 min at 4°C, washed once with 1 mL of ice cold 75% ethanol and air dried.

RNA pellets were resuspended in 12 μL water 1 μL of 3 μM cDNA and 1 μL of 10mM dNTPs and heated to 70°C for 5 min then rapidly cooled to 4°C. cDNA Master Mix (4 μL 5× Super Script IV (SSIV) Buffer, 1 μL 100mM DTT, 1 μL SSIV, 6 μL total) was added to the annealed RNA and incubated for 30min at 55°C. cDNA:RNA hybrids were captured by addition of 5 μL of MyOne Streptavidin C1 Dynabeads (Thermo Fisher Scientific) that had been rinsed and suspended in 50 μL of Biotin-IP buffer (100 mM Tris, pH 7.5, 1M NaCl, 1 mM EDTA, 0.1% Tween), and end over end rotation for 45 min at room temperature. Beads were placed on a 96-well magnet and washed sequentially twice with 100 μL of Biotin IP buffer and 100 μL ice-cold 1×PBS. Beads were resuspended in 10 μL of cDNA elution buffer (8.25 μL water, 1 μL of 1 μM P3 short oligo, and 0.75 μl of 50 mM $MnCl_2$) and heated to 95°C for 10 minutes, ramp 0.1 degree/second to 60°C forever. Next 5 μL of circularization reaction buffer (3.3 μL water, 1.5 μL 10× Circligase-II buffer, and 0.5 μL of Circligase-II (Epicentre)) was added. cDNA was circularized for 2 hours at 60°C. cDNA was purified with 30 μL of AMPure XP beads (Beckman Coulter) and 75 μL of isopropanol. Samples were incubated for 20 minutes at 25°C, washed twice with 100 μL 80% ethanol, air dried for 5 minutes, and eluted in 14 μL of water. Elution took place at 95°C for 3 minutes and immediately transferred to a 96-well magnet. Eluted cDNA was transferred to a new PCR tube containing 15 μL of 2× Phusion HF-PCR Master Mix (NEB), 0.5 μL of 30 μM P3/P6 PCR oligo mix and 0.5 μl of 15× SYBR Green I (Thermo Fisher Scientific). Real-time quantitative PCR was performed: 98°C 2 min, 15 cycles of 98°C 15 seconds, 65°C 30 seconds, 72°C, 30 seconds, with data acquisition set to the 72°C extension. PCR1 reactions were cleaned up by adding of 4.5 μL of isopropanol, 54 μL of AMPure XP beads and incubation for 10 min. Beads were washed once with 80% ethanol, dried for 5 min, and eluted in 15 μl of water. Illumina flow cell adaptors were added by adding 15 μL 2× Phusion HF-PCR Master Mix and 0.4 μL P3solexa/P6solexa oligo mix and amplified: 98°C 2 min, 3

cycles of 98°C 15 seconds, 65°C 30 seconds, 72°C, 30s seconds. Final libraries were purified by addition of 48 μL of AMPure XP beads and incubation for 5 min. Beads were washed twice with 70% ethanol, dried for 5 min, and eluted in 20 μL of water. 1–2μL of libraries were quantitated by HS-DNA Bioanalyzer. Samples were deep sequenced on the Illumina NextSeq machine: single-end, no index, high-output, 75-bp cycle run.

Analysis of irCLIP data

irCLIP data was processed using the FAST-iCLIP pipeline (https://github.com/ChangLab/FAST-iCLIP/tree/lite). PCR duplicates were removed using unique molecular identifiers in the RT primer region. Adapter and barcode sequences were trimmed, and reads were mapped step-wise to, viral (DENV or ZIKV), repetitive, and finally non-repetitive (GRCh38) genomes. Bowtie2 indexes were generated using the 'bowtie2-build' command in bowtie2 for DENV (KU725663.1) and ZIKV (KU501215.1) RNA genome sequences. Specific parameters used for the FAST-iCLIP pipeline are as follows: -f 18 (trims 17nt from the 5' end of the read), -l 16 (includes all reads longer than 16nt), –bm 29 (minimum MAPQ score from bowtie2 of 29 is required for mapping; unique mapping only), and –tr 2,3 (repetitive genome) and –tn 2,3 (non-repetitive genome) RT stop intersection (n,m; where n = replicate number and m = number of unique RT stops required per n replicates). Using the –tr/tn 2,3 parameters, a minimum of 6 RT stops are required to support any single nucleotide identified as crosslinking site. For gene ontology analysis, the top 25% of irCLIP bound genes were analyzed using the DAVID tool (https://david.ncifcrf.gov/tools.jsp). Peaks of RT stops were called on the biological replicated intersection of RT stop positions using iCount peaks (http://icount.readthedocs.io/en/latest/). The command line was as follows: iCount peaks gencode.v21.annotation.segment.gtf RTstop_input.bed Out_iCpeaks.bed --scores Out_iCpeaksScores.tsv. Regions from "Out_iCpeaks.bed" were then annotated with HOMER (http://homer.ucsd.edu/homer/) using the following command: annotatePeaks.pl Out_iCpeaks.bed hg38 > Out_iCpeaks_hg38_HOMERanno.txt -annStats Out_iCpeaks_hg38_HOMERanno_stats.txt.

CLIP Mass Spec (CLIPms)

Cells were grown, UV crosslinked, lysates generated, RNase A treated, IP'ed, and washed as described above for irCLIP. No dephosphorylation or RNA ligation took place, but RBP-RNA complexes were denatured and run in SDS-PAGE gels as per the irCLIP procedure above. After complete running of the SDS-PAGE, the gel was fixed and stained with the Colloidal Blue Staining Kit (Thermo Fisher Scientific) as per the manufacturer's instructions. Stain gels were visualized with the Odyssey CLx scanner and regions of each lane were excised based on where the predicted RBP-RNA complex would migrate.

Gel slices were prepared for mass spectrometry by rinsing sequentially in 200 μL HPLC-grade water, 100% Acetonitrile (ACN, Thermo Fisher Scientific), 50 mM Ammonium Bicarbonate (AmBic). Samples were reduced by adding 200 μL of 5 mM DTT in 50 mM AmBic and incubating at 65°C for 35 minutes. The reduction buffer was discarded and samples were cooled to room temperature. Alkylation was achieved by adding 200 μL of 25 mM iodoacetamide in 50 mM AmBic for 20 minutes at 25°C in the dark. The alkylation buffer was discarded, samples were rinsed once in 200 μL 50 mM AmBic, and then they

were washed twice for 10 minutes each in 200 μL of freshly prepared 50% ACN in 50 mM AmBic. After each wash, the supernatant was discarded, and after all washes, samples were dried for 3 hours using a SpeedVac. Once dry, proteins were digested by adding 100 ng of trypsin in 200 μL of 50 mM AmBic for 16 hours at 37°C. Samples were subsequently acidified by adding formic acid to a final concentration of 2.5% and incubating at 37°C for 45 minutes. Finally, samples were desalted using HyperSep Filter Plates with a 5–7 μL bed volume (Thermo Fisher Scientific) following the manufacturer's instructions. Samples were eluted three times in 100 μL 80% ACN in 2.5% formic acid, dried on a SpeedVac, and resuspended in 10 μL 0.1% formic acid for mass spectrometry analysis. Desalted peptides were analyzed by online capillary nanoLC-MS/MS. Samples were separated using a 20 cm reversed phase column fabricated in-house (100 μm inner diameter, packed with ReproSil-Pur C18-AQ 3.0 μm resin (Dr. Maisch GmbH)) that was equipped with a laser-pulled nanoelectrospray emitter tip. Peptides were eluted at a flow rate of 400 nL/min using a two-step linear gradient of 2–25% buffer B in 70 min and 25–40% B in 20 min (buffer A: 0.2% formic acid and 5% DMSO in water; buffer B: 0.2% formic acid and 5% DMSO in acetonitrile) in an Eksigent ekspert nanoLC-425 system (AB Sciex). Peptides were ionized with electrospray ionization into an Orbitrap Elite Hybrid Ion Trap-Orbitrap Mass Spectrometer (Thermo Fisher Scientific). Instrument method parameters were as follows: MS1 resolution, 60,000 at 400 m/z; scan range, 340−1600 m/z. The top 20 most-abundant ions were subjected to collision-induced dissociation with a normalized collision energy of 35%, activation q 0.25, and precursor isolation width 2 m/z. Dynamic exclusion was enabled with a repeat count of 1, a repeat duration of 30 seconds, and an exclusion duration of 20 seconds. FASTA sequences of the DENV (Accession Number: ANG57776) or ZIKA (Accession Number: AOR51315) proteomes were downloaded and appended to the human proteome (UniProt: UP000005640) for each database search. RAW files were searched using Byonic (Protein Metrics) with the following parameters: semi-specific cleavage specificity at the C-terminal site of R and K, allowing for 2 missed cleavages, precursor mass tolerance of 12 ppm, and fragment ion mass tolerance of 0.4 ppm. Methionine oxidation, asparagine deamidation, and N-term acetylation were set as variable modifications. Cysteine carbamidomethylation was set as a fixed modification. Peptide hits were filtered using a 1% FDR.

A custom Python script was written to merge technical and biological replicates across the different ChIRP-MS experiments (https://github.com/jasonkli/MS-Analysis). First, .xls output files from Byonic were analyzed for spectra of each protein identified. The total number of spectra, excluding any spectra with a quality score of less than 100, were counted and printed into new .xls files, one for each set of experiments. For each set of technical replicates, the number of spectra for each protein is summed across replicates and normalized by dividing by the total number of spectra from all reads in the set. These normalized values were then scaled factor of 1000 for readability. Next, we consolidated data across biological replicates. We filtered identified proteins such that a given protein was required to be present with at least 1 spectrum in each biological replicate. The normalized spectra of surviving protein ID's were then averaged across the biological replicates. Finally, a combined table was generated across all experimental data as generated by the previous steps. For each protein identified, we output the following information: common gene name,

UniProt ID, comma separated values of the raw spectra from each technical and biological replicate, the average normalized spectra from each experiment (with an added correction factor of 1 to avoid any 0's for subsequent analysis), the averaged normalized spectra divided by the number of amino acids in the protein, and the total amino acids in that protein.

Comprehensive identification of RNA binding proteins by mass spectrometry

DENV, ZIKV, and RV targeting probe were designed using online tools available at (https://www.biosearchtech.com/stellaris), with repeat masking setting of 3 and even coverage of the whole transcript. Full probe sequences are available in Supplementary Table 1. Oligos were synthesized with 3′ biotin-TEG modification at Stanford Protein and Nucleic Acid Facility (panoligo@stanford.edu).

ChIRP-MS was performed largely as described in Chu et al. 2015. 9× 7.5 million Huh7.5.1 were seeded and infected next day with either, DENV-2 (16681 strain-Hap1 adapted) or ZIKV PRVABC59 MOI 0.1 or Mock-treated in triplicate (3×3= 9 flasks/condition). For RV, 2× 7.5 million H1-HeLa cells were seeded and infected the next day at MOI 1 or mock infected. 48 hours after infection, media was aspirated, cells were rinsed once with 10ml of 1× PBS/Flask, trypsinized, pelleted at 1400 rpm for 5 min, washed twice with PBS. Cells were then resuspended in 3% formaldehyde containing PBS and rocked for 30 minutes at 25°C. Chemical crosslinking was then stopped by the addition of glycine to a final concentration of 125 mM for 5 minutes at 25°C. Crosslinked cells were pelleted at 2000 rpm for 5 minutes, supernatant discarded, and flash frozen at −80°C for storage. Lysate was generated by resuspending cell pellets in 1 mL lysis buffer (50 mM Tris-HCl pH 7.0, 10 mM EDTA, 1% SDS) per 100 mg of cell pellet weight (~100 μL pellet volume). Lysates were sonicated using a focused-ultrasonicator (Covaris, E220) until the average RNA length was 500 nucleotides as determined by agarose gel analysis and stored at −80°C. Stored lysates were thawed on ice, and for every 1 mL of sonicated lysate 2 mL of ChIRP hybridization buffer (750 mM NaCl, 1% SDS, 50 mM Tris-HCl pH 7.0, 1 mM EDTA, 15% formamide; made fresh) and precleared by adding 30 μL washed MyOne C1 beads per mL of lysate at 37°C for 30 minutes on rotation. Beads were removed twice from lysate using a magnetic stand; for this and all subsequent magnetic stand steps allow for > 1 minutes of separation before removing any supernatant. Next 1.5 μL of 100 μM ChIRP Probe Pools were added per mL of lysate. ChIRP Probe Pools (Supplementary Table 1) for Control (NI), DENV, or ZIKV enrichments were made by mixing equal volumes of 99 (DENV+ZIKV), 50 (DENV), or 49 (ZIKV) individual antisense oligos at 100 μM (final concentration of 1.01, 2, or 2.04 μM of each probe, respectively). The RV pool was made by mixing equal volumes of 50 individual antisense oligos targeting the RV genome at 100 μM (final concentration 2 μM of each probe) and was used for the RV-uninfected control. After mixing, hybridization took place on rotation for 16 hours at 37°C. Subsequently, 150 μL of washed MyOne C1 beads per mL of lysate were added to each sample and incubated on rotation for 45 minutes at 37°C. Enriched material was collected on the beads with a magnetic stand, and beads were washed 5× 2 minutes in 1 mL of ChIRP Wash Buffer (2× NaCl-Sodium Citrate (SSC, Thermo Fisher Scientific), 0.5% SDS) at 37°C. To elute enriched proteins, beads were collected on magnetic stand, resuspended in ChIRP biotin elution buffer (12.5 mM biotin,

7.5 mM HEPES, pH 7.9, 75 mM NaCl, 1.5 mM EDTA, 0.15% SDS, 0.075% sarkosyl, and 0.02% Na-Deoxycholate), mixed at 25°C for 20 min on rotation and at 65°C for 15 minutes shaking. Eluent was transferred to a fresh tube, and beads were eluted again. The two eluents were pooled (~1200 μL), and residual beads were removed again using the magnetic stand. 25% total volume (300 μL) trichloroacetic acid was added to the clean eluent, vortexed, and then samples were placed at 4°C overnight for precipitation. The next day, proteins were pelleted at 21,000 rcf at 4°C for 45 minutes. Supernatant was carefully removed and protein pellets were washed once with ice-cold acetone. Samples were spun at 21,000 rcf at 4°C for 5 minutes. Acetone supernatant was removed, tubes briefly centrifuged again and, after removal of residual acetone, were left to air-dry on bench-top. Proteins were then solubilized in 1× LDS Buffer in NT2 with 20 mM DTT and boiled at 95°C for 30 min with occasional mixing for reverse-crosslinking.

Protein samples were size-separated on bis-tris SDS-PAGE gels (Bio-Rad), fixed and stained with colloidal blue, and prepared for Mass Spec analysis as described above for CLIPms. For each NI, DENV, or ZIKV ChIRP-MS, biological triplicates were performed. Each replicate was cut into 4 slices in the SDS-PAGE and prepared independently (total of 4 MS runs per biological replicate). For RV ChIRP-MS, one replicate of RV-infected and non-infected H1-HeLa cells was used and split across 4 independent gel slices. ChIRP-MS data was searched with Byonic and processed as per the custom python script described above for CLIPms. Principal component analysis of the individual biological replicates was accomplished using the ClusterVis Tool (http://biit.cs.ut.ee/clustvis/)49. High confidence host factors associated with vRNAs were defined as being enriched greater than 2-fold over the non-infected cell ChIRP. To apply a statistical confidence filter to refine the ChIRP-MS hits, we used the SAINT scoring system[50] specifically the SAINTq software (http://saint-apms.sourceforge.net/Main.html). Individual biological triplicates for mock, DENV, or ZIKV infected ChIRP-MS hits were used as input data for the SAINTq software with default settings were for FDR calculations.

ChIRP-qRT-PCR

Cells were grown, infected, crosslinked, and sonicated as described above. After sonication, 1% of the lysate was removed and saved as an “input” sample. Lysates were again processed as above for preclearing, hybridization, MyOneC1 capture, and bead washing. After washing, 1% of each sample was removed as an “enriched” fraction. Enriched fractions were collected while the MyOneC1 beads were fully resuspended in ChIRP Wash Buffer. The input and enriched samples were brought to 95 μL in ChIRP PK buffer (10 mM Tris-HCl pH 7.0, 100 mM NaCl, 1 mM EDTA, 0.2% SDS) and to this 5 μL of 20 mg/mL Proteinase K. Protein was digested while shaking at 55°C for 45 minutes. RNA was extracted by adding 500 μL of TRIzol (Thermo Fisher Scientific), incubating at 55°C for 5 minutes, and then adding 100 μL chloroform. After mixing samples by vortexing for 7 seconds each, samples were incubated at 25°C for 5 minutes and then spun at 12,000 rpm at 4°C for 15 minutes. The aqueous layer was carefully removed from each sample, mixed with 2 volumes of 100% ethanol, and purified using a RNA Clean & Concentrator-25 (Zymo Research) as per the manufacturer’s instructions. All RNA samples were DNase-treated with the Turbo DNA-Free kit (Thermo Fisher Scientific). cDNA was generated using SuperScript VILO (Thermo

Fisher Scientific) according to manufacturer instructions. qPCR analyses were performed on the CFX96 Touch Real-Time PCR Detection System (Bio-Rad). All primers used are shown in Supplementary Table 1.

ChIRP and RNA-Bioanalyzer

Cells were grown, infected, and RNA harvested as described above. This RNA was either analyzed direction using the RNA Pico Bioanalyzer chip (Agilent Technologies) or analyzed using denaturing gel electrophoresis. A formaldehyde-agarose gel was made using the NorthernMax Kit (ThermoFisher Scientific) as per the manufactures protocol. RNA samples were denatured in 0.5× Gel Loading Buffer II (ThermoFisher Scientific) and 1× SybrGold (ThermoFisher Scientific) at 55°C for 10 minutes, cooled on ice for 3 minutes, and then loaded into the gel. After running at 110V for 35 minutes, RNA was imaged using a UV transilluminator.

RNA-seq from irCLIP samples

Input material for RNA-seq was obtained from the same lysates generated for the irCLIP experiment. After lysis and sonication, as described above, 100 μL of lysate from each biological duplicate of the non-infected, DENV, or ZIKV infected cells was taken. Proteins were digested and RNA extracted with Proteinase K and TRIzol as described in the “ChIRP-qRT-PCR” section. Ribosomal RNA was depleted using the RiboMinus Transcriptome Isolation Kit, human/mouse (Thermo Fisher Scientific) as per the manufactures instructions starting with 5 μg of total RNA per sample. rRNA-depleted samples were fragmented using the RNA Fragmentation Reagent (Thermo Fisher Scientific) at 90°C for 30 seconds. After fragmentation, the RNA samples were purified using a RNA Clean & Concentrator-5 (Zymo Research) as described in the “ChIRP-qRT-PCR” section, eluted the RNA in 5 μL of water. RNA 3’-ends were repaired by added 0.5 μL 10× T4-PNK buffer (New England Biolabs), 1 μL T4-PNK, 1 μL FastAP (Thermo Fisher Scientific), 1 μL of RiboLock (Thermo Fisher Scientific), and 1.5 μL of water for 45 minutes at 37°C. Next, a 3’-adaptor was ligated to the RNA samples by directly adding 1 μL 10× T4-RNL1 Buffer (New England Biolabs), 1 μL T4-RLN1 (New England Biolabs), 1 μL 100mM DTT, 0.75 μL 3 μM irCLIP 3’-adaptor and 6 μL 50% PEG8000 (New England Biolabs) for 4 hours at 25°C. After the ligation reaction completed, non-ligated 3’-adaptor was digested by directly adding 2.5 μL Rec-Jf (New England Biolabs), 1.25 μL 5’-deadenylase (Epicentre), 3 μL 10× 5’-deadenylase buffer (Epicentre), and incubating for 1 hour 37°C. Samples were purified using a RNA Clean & Concentrator-5 (Zymo Research) as above. Ligated and purified RNA samples were processed further into dsDNA libraries as per the final steps of the irCLIP procedure as described above. After library quantification and pooling, samples were sequenced on the NextSeq 500 platform (Illumina). Data was processed for mapping as per the irCLIP pipeline, however after mapping RT stops were not isolated. Instead the featureCount tool of the Subread package (version 1.6.0) was used to count aligned reads supporting transcripts annotated from Gencode Release 26 (GRCh38, https://www.gencodegenes.org/releases/26.html). Genes supported by at least 10 reads in a biological replicate were considered as expressed. RNA-seq counts were normalized by the total counts for all expressed genes in each sample to produce counts per million (CPM) reads. To calculate enrichment of ER annotated genes, a CPM cut-off of 1.0 was set for genes identified in the non-infected RNA-

seq (18199) and then intersected with ER annotated gene names from Uniprot (Supplementary Table 4). A two-sided Fisher's exact test was used to determine statistical enrichment.

Immunofluorescence and RNA Fluorescence in situ hybridization

Huh7.5.1 cells (80,000) were seeded on poly-lysine coated glass cover slips in 24 well format. The next day, cells were infected with either DENV-2 or ZIKV (Puerto Rico) at an MOI of 1 for 24 hours. Cells were fixed with 4% formaldehyde (Sigma), washed with PBS, and permeabilized using the Immunofluorescence Application Solution kit according to the manufacturer's recommendation (Cell Signaling, 12727. The ER-GFP marker was transfected into Huh7.5.1 cells using Lipofectamine 3000 (Thermo Fisher Scientific) according to manufacturer's guideline. At 48 hours post-transfection, cells were fixed with 4% formaldehyde for 30 minutes at room temperature, washed with PBS, and permeabilized with 1% NP-40 for 5 minutes at room temperature. Cells were stained using antibodies against RRBP1 (Bethyl, A303–996A, 1:100 dilutions), vigilin (Bethyl, A303–971A, 1:20 dilutions), GFP (Thermo Fisher Scientific, MA5–15256, 1:100 dilutions) for 90 minutes at room temperature. Cells were washed twice with PBS and stained with secondary Alexa Fluor antibodies 488nm, 594nm, 647nm (Thermo Fisher Scientific #A-11034, #R37117, #A31573) at 1:200 dilutions for 1 hour at room temperature. RNA probes that detect the positive strand vRNA for DENV and ZIKV were purchased from Affymetrix. Viral RNAs were then stained using RNA probes in conjunction with bDNA amplification to generate single molecule detection of viral RNA as per the manufacturer's protocol (ViewRNA Cell Plus Assay #88–19000-99). Finally, coverslips were mounted onto glass slides using PermaFluor (Thermo Fisher Scientific) containing DAPI (Affymetrix). Cells were visualized on a Nikon AR1 or a Leica SP8 confocal microscope. At least 30 cells were analyzed for each condition using ImageJ colocalization algorithm COLOC2 (https://github.com/fiji/Colocalisation_Analysis/releases/tag/Colocalisation_Analysis-3.0.0). Pearson's correlation scores for colocalization were plotted to determine the level of colocalization between viral RNAs and either the costained host proteins or DAPI.

Sub-cellular Fractionation

300,000 Huh7.5.1 cells were washed twice with cold PBS. Cells were then separated into their cytosolic and ER compartments as previously described[24]. Briefly, the cytosol fraction was extracted by addition of a buffer containing 0.03% digitonin, 110 mM KOAc, 25 mM K-HEPES pH 7.2, 15 mM $MgCl_2$, and 4 mM $CaCl_2$ to the dish and incubated on ice for 5 minutes. The supernatant with the buffer containing the cytosolic contents was collected after low speed centrifugation (600 rcf for 5 minutes) and cells washed with the same buffer containing 0.0015% digitonin. The first lysis and the wash were combined and represent the cytosolic contents of the cell. The membrane fraction which contains ER membranes was then collected by lysis of the digitonin-extracted cell pellet with an ER lysis buffer containing 2% n-dodecyl-β-D-maltoside, 200 mM KOAc, 25 mM K-HEPES pH 7.2, 15 mM $MgCl_2$, and 4 mM $CaCl_2$. Western blot analysis from the two different fractions was then performed with antibodies against RRBP1, vigilin, the cytoplasmic markers GAPDH (Genetex GTX 627408) and tubulin (Abcam ab97872) and the ER marker RPN1 (Bethyl Laboratories A305–026A).

Native co-IP

Huh7.5.1 cells were seeded in 6-well plates and infected with DENV-2 at MOI of 0.1 or no virus (NI) as described above. Protein G beads were pre-conjugated to rabbit-IgG (Thermo Fisher Scientific, 02–6102) or anti-RRBP1 (Bethyl, A303–996A) antibodies; 3 μg antibody and 10 μL Protein G beads per IP reaction. After 48 hours of infection, protein lysate was generated by adding 650 μL of co-IP lysis buffer (10 mM HEPES, 2 mM $MgCl_2$, 10 mM KCl, 0.5% NP-40, 0.5 mM EDTA, 150 mM NaCl) to each well, disrupting the cells with a cell lifter, incubating the lysate at 4°C for 30 min. Lysates were cleared by spinning at 4°C for 5 min at 5200 rcf. 100 μL of clarified lysate from NI or DENV2 infections were diluted in 400 μL co-IP lysis buffer (final 500 μL) to which the pre-conjugated antibody-Protein G beads were added for 3 hours at 4°C on rotation. Each condition was performed in biological triplicate. RNase-treated samples were generated by adding 1 μL of 1 μg/μL RNase A to the lysate during the IP at 4°C. After 3 hours, each sample was washed 3× 750 μL of co-IP lysis buffer and 1× 750 μL NT2 buffer. Enriched proteins were subsequently analyzed by western blotting.

Genome-scale CRISPR/Cas9 knockout screens

Genome-scale CRISPR/Cas9 mutagenized Huh7.5.1 cells were generated as previously described [16,51]. In brief, stable Cas9 expressing Huh7.5.1 WT cells were engineered by transducing lentiCas9-Blast and selected using blasticidin. Subsequently, 300 million Cas9 expressing Huh7.5.1 cells were transduced with the lentiGuide-Puro from the GeCKOv2 library [51] at an MOI of 0.3. Puromycin-resistant cells were selected, pooled, and expanded. These mutagenized cells were ready to be used for CRISPR genetic screens at 10 days post-transduction. 65 million mutagenized cells for each library (A and B) were seeded for 16 hours and then subjected to DENV infections: DENV-1^{276RKI} (MOI=0.4 PFU/cell), DENV-2^{429557} (MOI=0.05 PFU/cell), DENV-$3^{Philippines/H871856}$ (MOI=0.003 PFU/cell), and DENV-$4^{BC287/97}$ (MOI=0.1 PFU/cell). As soon as 4 days post-infection, cytopathic effects (CPE) were observed. Populations of virus-resistant cells were harvested between 19–24 days post-infection. Uninfected starting populations of mutagenized cells were used as the unselected reference. Total genomic DNA from both virus-resistant and uninfected cells was respectively extracted using QIAamp DNA Mini Kit (Qiagen). The inserted guide RNA sequences were retrieved from the genomic DNA by PCR amplification using primers F1 and R1 (Supplementary Table 1). The PCR products were further barcoded by an additional round of PCR amplification using specific primers listed in Supplementary Table 1. Barcoded PCR products were then purified and subjected to NextSeq platform (Illumina) next-generation sequencing (NGS) using a custom NGS primer (Supplementary Table 1). The sequencing data were processed and analyzed using MAGeCK algorithm to determine the ranking of each hit by taking the following criteria into account: the number of sequencing reads for each unique guide, the number of unique guide RNA per gene (i.e. 0–6), and the enrichment of a particular guide RNA in comparison to uninfected cell populations[52]. The separate NGS FASTQ files for all four DENV serotypes were concatenated into one file and subsequently subjected to MAGeCK analysis. For gene ontology (GO) analysis, the top 50 hits of pan-DENV serotypes CRISPR KO screens were analyzed using The Database for Annotation, Visualization and Integrated Discovery, DAVID[53] (https://david.ncifcrf.gov/tools.jsp).

Haploid genetic screens

The haploid genetic screens were performed as previously described[45,54]. Briefly, 3× 100 million gene-trap mutagenized HAP1 cells were seeded and infected with the following Zika Virus strains: $ZIKV^{FLR}$ (Colombia strain), $ZIKV^{PRVABC59}$, $ZIKV^{H/PF/2013}$ (MOI=1). Forty-eight hours post-infection media was aspirated and replaced with fresh IMDM containing 10% FBS. Clear cytopathic effects were observed at two and three days of infection leading to death of the majority of cells. Ten days after infection, resistant HAP1 colonies were harvested (yield ~30 million cells/virus strain) and genomic DNA was isolated. Gene-trap insertion sites were determined by linear amplification of the genomic DNA (gDNA) flanking regions of the gene-trap DNA insertion sites thanks to LAM-PCR. Briefly, genomic DNA from selected and unselected populations (~40 million cells per condition) were isolated using the QIAamp Mini Kit (Qiagen). The isolated genomic DNA was then digested by MseI and SpeI restriction enzymes separately and the resulting digested DNA products from both digestion reactions were pooled for each condition. A linear PCR using biotinylated primers recognizing the LTR (Supplementary Table 1) of the gene-trap was performed using the AccuPrime PCR kit from Invitrogen. A DNA linker primer (Supplementary Table 1) was then ligated to the LAM-PCR products on-beads using the Circligase II kit (Epicentre). Biotinylated PCR products were then isolated using magnetic streptavidin beads provided with the Dynal® kilobaseBINDER™ Kit (Invitrogen). Then a final PCR using primer sets with Solexa adaptor sequences (Supplementary Table 1) and bar codes were used to amplify isolated fragments with different sizes. Final PCR products were checked on a 2% agarose gel and sent to sequencing on an Illumina NextSeq platform. Reads were aligned to the human genome using Bowtie and enrichment of independent insertions was calculated as previously described [16]. *P*-value (corrected for false-discovery rate) for each gene identified in the screen was determined using one-sided Fisher's exact test run in the R software environment. If the *P*-value was lower than the R software could report, the corrected *P*-value was set to the smallest non-zero normalized floating-point number R could report, which is $\sim 1 \times 10^{-307}$(Ref ([54])). The screens were individually compared to the unselected dataset, or the fastq files were first merged to detect genes common to the three screens. For gene ontology (GO) analysis, the top 50 hits of ZIKV Haploid Genetic screens were analyzed using The Database for Annotation, Visualization and Integrated Discovery, DAVID (https://david.ncifcrf.gov/tools.jsp).

RNA stability and northern blot analysis

The 3'UTR of the DENV-2 16681 infectious clone (nucleotides 10,205–10,704) was PCR amplified (Supplementary Table 1) and Zero-Blunt cloned into pCR®-Blunt plasmid (Thermo Fisher Scientific). This plasmid served as a template to generate northern blot probes that hybridize to the 3'UTR of DENV-2. To prepare cell lysates for northern blot, 2 million cells (WT or RRBP1/vigilin-double KO) on 60-mm dish were first infected with DENV-2 (16681) at MOI of 0.25 PFU/cell for 48 h. At 48 hpi, the replication inhibitor MK0608 (at 50 μM final concentration) was introduced to infected cells for blocking further replication of DENV-2. At designated time points post MK0608 treatment, cells were washed twice with cold PBS and harvested in TRIzol (Thermo Fisher Scientific). Total RNA was extracted using the RNeasy Mini kit (Qiagen) following the manufacturers protocol. For northern blot analysis of Dengue vRNA, 10 μg of total RNA in RNA loading buffer (32%

formamide, 1× MOPS-EDTA-Sodium acetate (MESA, Sigma), and 4.4% formaldehyde) were denatured for 20 minutes at 70°C, separated in a 1.2% agarose gel containing 1× MESA and 3.7% formaldehyde, transferred overnight and UV-crosslinked to a Zeta-probe membrane (Bio-Rad). The membrane was blocked and hybridized using ExpressHyb hybridization buffer (Clontech) and $\alpha-^{32}$P dATP-RadPrime DNA labeled probes. Densitometry analysis of the bands was performed using the ImageJ open access software.

Supplementary Material

Refer to Web version on PubMed Central for supplementary material.

Acknowledgements

We would like to thank A. Rubin, O. Botvinnik, M.R. Corces, and A. Za for helpful discussions with statistical and computational analyses. J. Ule, J. Zmrzlikar, and N Haberman for help with the iCount peak calling software. L. Zhang and the Elias lab for assistance running samples for MS analysis. J. Coller, X. Ji, and D. Wagh, and the Stanford Functional Genomics Facility for assistance running samples for deep sequencing. We also thank the Stanford shared FACS facility and its former director Marty Bigos for technical assistance. We acknowledge the NIH Biodefense and Emerging Infections Research Repository (BEI Resources), NIAID, NIH for providing multiple DENV and ZIKV strains mentioned in the Materials and Methods. We thank Simon Braun, members of the Carette, Kirkegaard, and Sarnow labs for helpful discussions and critical reading of the manuscript. The work was funded in part by the NIH (grants DP2 AI104557, R01 AI141970 and U19 AI109662 to J.E.C.; R37 AI047365 and R01 AI069000 to P.S.; R01 AI051622 to C.R.B.), the Burroughs Wellcome Investigators in the Pathogenesis of Infectious Disease (J.E.C.), the David and Lucile Packard Foundation (J.E.C.), the Stanford Dean's Fellowship (Y.S.O.), the Child Health Research Institute Stanford (K.M), the Damon Runyon Cancer Research Foundation (R.A.F), the NSF-GRF (A.G.J. and C.D.M), and the Howard Hughes Medical Institute (C.R.B). C.D.M., J.G., L.M. and M.E.B. were supported by the Intramural Research Program of NIAID.

References

1. Bhatt S et al. The global distribution and burden of dengue. Nature 496, 504–507, doi:10.1038/nature12060 (2013). [PubMed: 23563266]
2. Shepard DS, Undurraga EA, Halasa YA & Stanaway JD The global economic burden of dengue: a systematic analysis. Lancet Infect Dis 16, 935–941, doi:10.1016/S1473-3099(16)00146-8 (2016). [PubMed: 27091092]
3. Kaufmann SHE, Dorhoi A, Hotchkiss RS & Bartenschlager R Host-directed therapies for bacterial and viral infections. Nat Rev Drug Discov 17, 35–56, doi:10.1038/nrd.2017.162 (2018). [PubMed: 28935918]
4. Puschnik AS et al. A Small-Molecule Oligosaccharyltransferase Inhibitor with Pan-flaviviral Activity. Cell Rep 21, 3032–3039, doi:10.1016/j.celrep.2017.11.054 (2017). [PubMed: 29241533]
5. Apte-Sengupta S, Sirohi D & Kuhn RJ Coupling of replication and assembly in flaviviruses. Curr Opin Virol 9, 134–142, doi:10.1016/j.coviro.2014.09.020 (2014). [PubMed: 25462445]
6. Fernandez-Garcia MD, Mazzon M, Jacobs M & Amara A Pathogenesis of flavivirus infections: using and abusing the host cell. Cell Host Microbe 5, 318–328, doi:10.1016/j.chom.2009.04.001 (2009). [PubMed: 19380111]
7. Walsh D & Mohr I Viral subversion of the host protein synthesis machinery. Nat Rev Microbiol 9, 860–875, doi:10.1038/nrmicro2655 (2011). [PubMed: 22002165]
8. Garcia-Blanco MA, Vasudevan SG, Bradrick SS & Nicchitta C Flavivirus RNA transactions from viral entry to genome replication. Antiviral Res 134, 244–249, doi:10.1016/j.antiviral.2016.09.010 (2016). [PubMed: 27666184]
9. Chu C et al. Systematic discovery of Xist RNA binding proteins. Cell 161, 404–416, doi:10.1016/j.cell.2015.03.025 (2015). [PubMed: 25843628]
10. Chen CK et al. Xist recruits the X chromosome to the nuclear lamina to enable chromosome-wide silencing. Science 354, 468–472, doi:10.1126/science.aae0047 (2016). [PubMed: 27492478]

11. Balinsky CA et al. IRAV (FLJ11286), an Interferon-Stimulated Gene with Antiviral Activity against Dengue Virus, Interacts with MOV10. J Virol 91, doi:10.1128/jvi.01606-16 (2017).
12. Paranjape SM & Harris E Y box-binding protein-1 binds to the dengue virus 3'-untranslated region and mediates antiviral effects. J Biol Chem 282, 30497–30508, doi:10.1074/jbc.M705755200 (2007). [PubMed: 17726010]
13. Umareddy I et al. Dengue virus regulates type I interferon signalling in a strain-dependent manner in human cell lines. J Gen Virol 89, 3052–3062, doi:10.1099/vir.0.2008/001594-0 (2008). [PubMed: 19008393]
14. Lei Y et al. Functional interaction between cellular p100 and the dengue virus 3' UTR. J Gen Virol 92, 796–806, doi:10.1099/vir.0.028597-0 (2011). [PubMed: 21148275]
15. Hentze MW, Castello A, Schwarzl T & Preiss T A brave new world of RNA-binding proteins. Nat Rev Mol Cell Biol 19, 327–341, doi:10.1038/nrm.2017.130 (2018). [PubMed: 29339797]
16. Marceau CD et al. Genetic dissection of Flaviviridae host factors through genome-scale CRISPR screens. Nature 535, 159–163, doi:10.1038/nature18631 (2016). [PubMed: 27383987]
17. Savidis G et al. Identification of Zika Virus and Dengue Virus Dependency Factors using Functional Genomics. Cell Rep 16, 232–246, doi:10.1016/j.celrep.2016.06.028 (2016). [PubMed: 27342126]
18. Zhang R et al. A CRISPR screen defines a signal peptide processing pathway required by flaviviruses. Nature 535, 164–168, doi:10.1038/nature18625 (2016). [PubMed: 27383988]
19. Lin DL et al. Dengue Virus Hijacks a Noncanonical Oxidoreductase Function of a Cellular Oligosaccharyltransferase Complex. MBio 8, doi:10.1128/mBio.00939-17 (2017).
20. Li J et al. A short hairpin RNA screen of interferon-stimulated genes identifies a novel negative regulator of the cellular antiviral response. MBio 4, e00385–00313, doi:10.1128/mBio.00385-13 (2013). [PubMed: 23781071]
21. Cui XA, Zhang H & Palazzo AF p180 promotes the ribosome-independent localization of a subset of mRNA to the endoplasmic reticulum. PLoS Biol 10, e1001336, doi:10.1371/journal.pbio.1001336 (2012). [PubMed: 22679391]
22. Mobin MB et al. The RNA-binding protein vigilin regulates VLDL secretion through modulation of Apob mRNA translation. Nat Commun 7, 12848, doi:10.1038/ncomms12848 (2016). [PubMed: 27665711]
23. Losfeld ME, Soncin F, Ng BG, Singec I & Freeze HH A sensitive green fluorescent protein biomarker of N-glycosylation site occupancy. FASEB journal: official publication of the Federation of American Societies for Experimental Biology 26, 4210–4217, doi:10.1096/fj.12-211656 (2012). [PubMed: 22691915]
24. Reid DW et al. Dengue Virus Selectively Annexes Endoplasmic Reticulum-Associated Translation Machinery as a Strategy for Co-opting Host Cell Protein Synthesis. J Virol 92, doi:10.1128/JVI.01766-17 (2018).
25. Zarnegar BJ et al. irCLIP platform for efficient characterization of protein-RNA interactions. Nat Methods 13, 489–492, doi:10.1038/nmeth.3840 (2016). [PubMed: 27111506]
26. Savitz AJ & Meyer DI Identification of a ribosome receptor in the rough endoplasmic reticulum. Nature 346, 540–544, doi:10.1038/346540a0 (1990). [PubMed: 2165568]
27. Eliseev B et al. Structure of a human cap-dependent 48S translation pre-initiation complex. Nucleic Acids Res 46, 2678–2689, doi:10.1093/nar/gky054 (2018). [PubMed: 29401259]
28. Belanger L, Roy S & Allard D New albumin gene 3' adjacent to the alpha 1-fetoprotein locus. J Biol Chem 269, 5481–5484 (1994). [PubMed: 7509788]
29. Shelness GS, Ingram MF, Huang XF & DeLozier JA Apolipoprotein B in the rough endoplasmic reticulum: translation, translocation and the initiation of lipoprotein assembly. J Nutr 129, 456S–462S, doi:10.1093/jn/129.2.456S (1999). [PubMed: 10064309]
30. Darnell JC et al. FMRP stalls ribosomal translocation on mRNAs linked to synaptic function and autism. Cell 146, 247–261, doi:10.1016/j.cell.2011.06.013 (2011). [PubMed: 21784246]
31. Chen YL, Yokokawa F & Shi PY The search for nucleoside/nucleotide analog inhibitors of dengue virus. Antiviral Res 122, 12–19, doi:10.1016/j.antiviral.2015.07.010 (2015). [PubMed: 26241002]
32. Cheng MH & Jansen RP A jack of all trades: the RNA-binding protein vigilin. Wiley Interdiscip Rev RNA 8, doi:10.1002/wrna.1448 (2017).

33. Cui XA & Palazzo AF Localization of mRNAs to the endoplasmic reticulum. Wiley Interdiscip Rev RNA 5, 481–492, doi:10.1002/wrna.1225 (2014). [PubMed: 24644132]
34. Cunningham KS, Dodson RE, Nagel MA, Shapiro DJ & Schoenberg DR Vigilin binding selectively inhibits cleavage of the vitellogenin mRNA 3'-untranslated region by the mRNA endonuclease polysomal ribonuclease 1. Proc Natl Acad Sci U S A 97, 12498–12502, doi:10.1073/pnas.220425497 (2000). [PubMed: 11050168]
35. Hyde M, Block-Alper L, Felix J, Webster P & Meyer DI Induction of secretory pathway components in yeast is associated with increased stability of their mRNA. J Cell Biol 156, 993–1001, doi:10.1083/jcb.200112008 (2002). [PubMed: 11901166]
36. Reid DW & Nicchitta CV Diversity and selectivity in mRNA translation on the endoplasmic reticulum. Nat Rev Mol Cell Biol 16, 221–231, doi:10.1038/nrm3958 (2015). [PubMed: 25735911]
37. Ueno T, Kaneko K, Sata T, Hattori S & Ogawa-Goto K Regulation of polysome assembly on the endoplasmic reticulum by a coiled-coil protein, p180. Nucleic Acids Res 40, 3006–3017, doi:10.1093/nar/gkr1197 (2012). [PubMed: 22156060]
38. Kruse C et al. The multi-KH protein vigilin associates with free and membrane-bound ribosomes. Cell Mol Life Sci 60, 2219–2227, doi:10.1007/s00018-003-3235-0 (2003). [PubMed: 14618268]
39. Batlle M, Marsellach FX, Huertas D & Azorin F Drosophila vigilin, DDP1, localises to the cytoplasm and associates to the rough endoplasmic reticulum. Biochim Biophys Acta 1809, 46–55, doi:10.1016/j.bbagrm.2010.10.005 (2011). [PubMed: 21035573]
40. Frey S, Pool M & Seedorf M Scp160p, an RNA-binding, polysome-associated protein, localizes to the endoplasmic reticulum of Saccharomyces cerevisiae in a microtubule-dependent manner. J Biol Chem 276, 15905–15912, doi:10.1074/jbc.M009430200 (2001). [PubMed: 11278502]
41. Hirschmann WD et al. Scp160p is required for translational efficiency of codon-optimized mRNAs in yeast. Nucleic Acids Res 42, 4043–4055, doi:10.1093/nar/gkt1392 (2014). [PubMed: 24445806]
42. Phillips SL, Soderblom EJ, Bradrick SS & Garcia-Blanco MA Identification of Proteins Bound to Dengue Viral RNA In Vivo Reveals New Host Proteins Important for Virus Replication. MBio 7, e01865–01815, doi:10.1128/mBio.01865-15 (2016). [PubMed: 26733069]
43. Viktorovskaya OV, Greco TM, Cristea IM & Thompson SR Identification of RNA Binding Proteins Associated with Dengue Virus RNA in Infected Cells Reveals Temporally Distinct Host Factor Requirements. PLoS Negl Trop Dis 10, e0004921, doi:10.1371/journal.pntd.0004921 (2016). [PubMed: 27556644]
44. Schoggins JW et al. A diverse range of gene products are effectors of the type I interferon antiviral response. Nature 472, 481–485, doi:10.1038/nature09907 (2011). [PubMed: 21478870]
45. Carette JE et al. Ebola virus entry requires the cholesterol transporter Niemann-Pick C1. Nature 477, 340–343, doi:10.1038/nature10348 (2011). [PubMed: 21866103]
46. Mlera L, Meade-White K, Saturday G, Scott D & Bloom ME Modeling Powassan virus infection in Peromyscus leucopus, a natural host. PLoS Negl Trop Dis 11, e0005346, doi:10.1371/journal.pntd.0005346 (2017). [PubMed: 28141800]
47. Shan C et al. An Infectious cDNA Clone of Zika Virus to Study Viral Virulence, Mosquito Transmission, and Antiviral Inhibitors. Cell Host Microbe 19, 891–900, doi:10.1016/j.chom.2016.05.004 (2016). [PubMed: 27198478]
48. Lanke KH et al. GBF1, a guanine nucleotide exchange factor for Arf, is crucial for coxsackievirus B3 RNA replication. J Virol 83, 11940–11949, doi:10.1128/JVI.01244-09 (2009). [PubMed: 19740986]
49. Metsalu T & Vilo J ClustVis: a web tool for visualizing clustering of multivariate data using Principal Component Analysis and heatmap. Nucleic Acids Res 43, W566–570, doi:10.1093/nar/gkv468 (2015). [PubMed: 25969447]
50. Teo G et al. SAINTq: Scoring protein-protein interactions in affinity purification - mass spectrometry experiments with fragment or peptide intensity data. Proteomics 16, 2238–2245, doi:10.1002/pmic.201500499 (2016). [PubMed: 27119218]
51. Sanjana NE, Shalem O & Zhang F Improved vectors and genome-wide libraries for CRISPR screening. Nat Methods 11, 783–784, doi:10.1038/nmeth.3047 (2014). [PubMed: 25075903]

52. Li W et al. MAGeCK enables robust identification of essential genes from genome-scale CRISPR/Cas9 knockout screens. Genome Biol 15, 554, doi:10.1186/s13059-014-0554-4 (2014). [PubMed: 25476604]

53. Huang da W, Sherman BT & Lempicki RA Systematic and integrative analysis of large gene lists using DAVID bioinformatics resources. Nature protocols 4, 44–57, doi:10.1038/nprot.2008.211 (2009). [PubMed: 19131956]

54. Carette JE et al. Global gene disruption in human cells to assign genes to phenotypes by deep sequencing. Nat Biotechnol 29, 542–546, doi:10.1038/nbt.1857 (2011). [PubMed: 21623355]

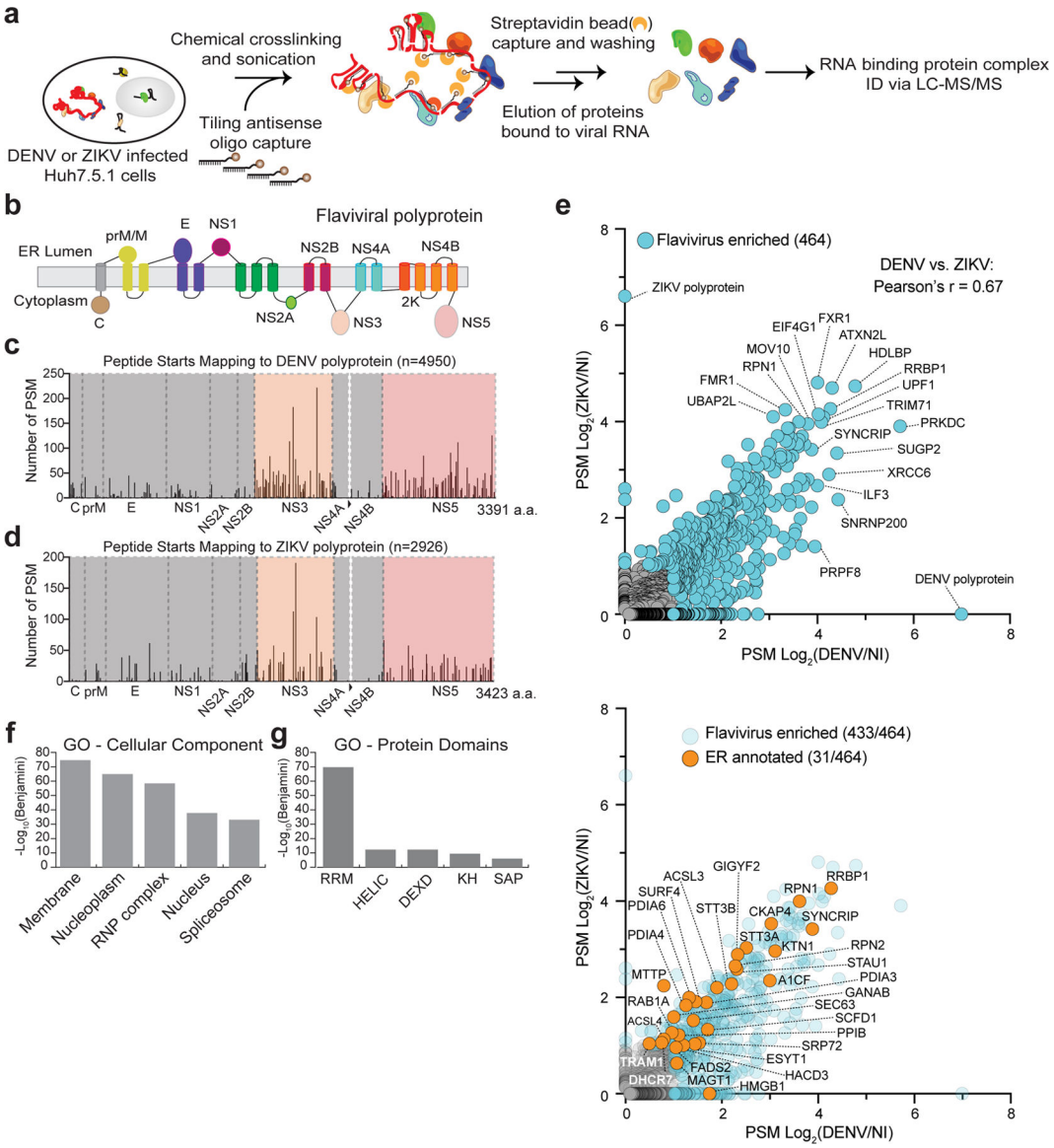

Fig. 1. ChIRP-MS reveals the protein interactome of DENV and ZIKV RNA genomes.

a, Outline of the ChIRP-MS method. Uninfected, DENV, or ZIKV infected Huh7.5.1 cells were formaldehyde crosslinked and solubilized by sonication. Target viral RNA was pulled-down by biotinylated anti-sense oligonucleotides, associated proteins were eluted, and subjected to LC-MS/MS. **b**, Cartoon of the topology of the flaviviral polyprotein inserted in the ER membrane. **c**, and **d**, Map of DENV (**c**) and ZIKV (**d**) genome organizations with corresponding MS spectral counts determined by ChIRP-MS. **e**, Scatter plot depicting enrichment ratio of host proteins identified by ChIRP-MS with DENV and ZIKV RNA over uninfected background. ChIRP-MS was performed in triplicates for each virus and x- and y-axis represent the mean of Peptide Spectrum-Matches (PSM) scores enrichment over background for DENV and ZIKV, respectively. A total number of 464 enriched proteins were identified for DENV and ZIKV and several of the most enriched hits are indicated in the top panel. The bottom panel demonstrated that 3¼64 enriched proteins are ER-annotated

proteins and the remaining 43¾64 proteins are implicated in other non-ER sub-cellular localizations. A full list of the enriched proteins is presented in Supplementary Table 2. **f**, GO cellular component analysis of high confidence host factors enriched by ChIRP-MS. **g**, GO protein domain analysis of high confidence host factors enriched by ChIRP-MS. For panel **f** and **g**, FDR calculation was performed using the Benjamini Hochberg method on the combined ChIRP-MS enriched hits (n = 1 merged dataset).

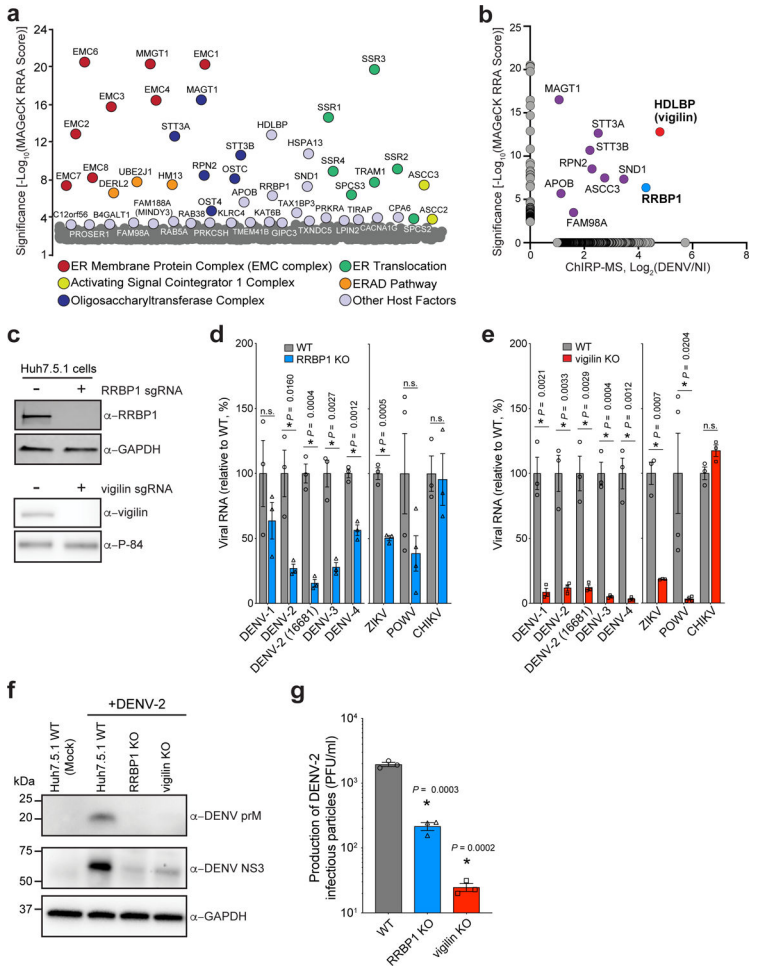

Fig. 2. Intersection of ChIRP-MS with genome-wide CRISPR screens nominates functionally relevant pro-viral host proteins.

a, Genome-scale CRISPR knockout screens for all four DENV serotypes (DENV-1^{276RKI}, DENV-2^{429557}, DENV-3$^{Philippines/H871856}$, and DENV-4$^{BC287/97}$) in Huh7.5.1 cells. The genetic screens were independently performed for each serotype, analyzed with MAGeCK, and combined to obtain significance scores (y-axis). The 50 most enriched genes were colored and grouped by function. **b**, Scatter plot depicting enrichment scores of high-confidence ChIRP-MS DENV hits (x-axis) and the 200 top scoring hits from DENV CRISPR genetic screens (y-axis). Common hits shared by both DENV genetic screens and DENV ChIRP-MS were colored in red (vigilin), blue (RRBP1), and purple (others). **c**, Western blot (WB) analysis of wild-type (WT) or clonal RRBP1 knock-out (KO) (upper panel) and vigilin-KO (lower panel) cells in Huh7.5.1 cells. Representative WB of $n = 2$ biologically independent replicates showing similar results. **d**, qRT-PCR analysis of DENV infected WT and RRBP1-KO Huh7.5.1 cells (48 hours post-infection (hpi), MOI of 0.1) or ZIKV^{PRVABC59}, POWV^{LB} (48 hpi, MOI 0.1) and CHIKV$^{181/25}$ (24 hpi, MOI of 0.01) infected WT and RRBP1-KO Huh7.5.1 cells. **e**, qRT-PCR analysis as in (**d**) here with vigilin-KO. Note: The WT datasets for POWV in panel **d** and **e** derived from the same experiments. **f**, WB analysis of DENV-2^{429557} infected (MOI of 0.1, 72 hpi) WT, RRBP1-KO, and vigilin-KO Huh7.5.1 cell lysates, probed with DENV prM and NS3 antibodies.

Representative WB of $n = 4$ biologically independent replicates showing similar results. **g**, Titers of infectious particles production from WT, RRBP1-KO, and vigilin-KO Huh7.5.1 cells infected with DENV-2^{429557} at MOI of 0.1 for 72 h. For panel **d**, **e**, and **g,** the datasets represent the mean with standard error of the mean (SEM) of $n = 3$ independent biological replicates, except for POWV, $n = 4$ independent biological replicates. All *P*-values were determined by two-tailed, unpaired *t*-test using GraphPad Prism (GraphPad Software), where * = $P < 0.05$ and n.s. = non-significant.

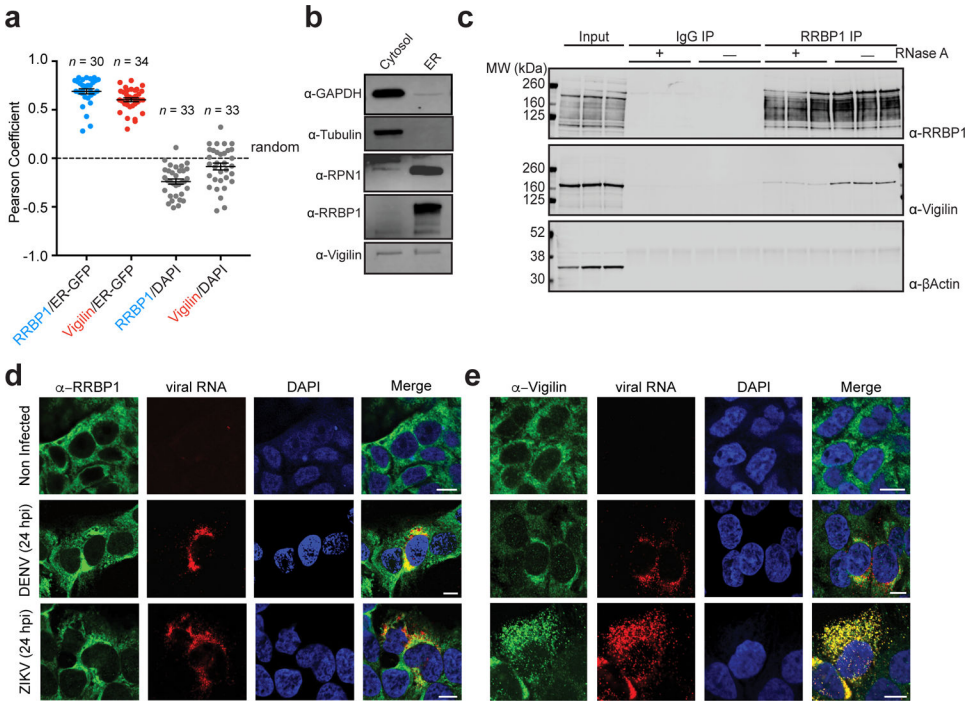

Fig. 3. RRBP1 and vigilin interact at the endoplasmic reticulum.

a, Single cell quantification and correlation between, RRBP1, vigilin, ER-GFP (an ER marker), and 4′,6-diamidino-2-phenylindole (DAPI) immunofluorescence signals. Total number of cells that were randomly chosen for each analysis, with mean and SEM are indicated. **b**, Western blot analysis of ER and cytosolic cell fractions probed with GAPDH or Tubulin (cytosolic markers), RPN1 (ER marker), RRBP1, and vigilin antibodies. Representative WB of $n = 3$ biologically independent replicates showing similar results. **c**, Western blot analysis of three independent co-IP experiments from non-infected Huh7.5.1 cells with RRBP1 as the bait showing similar results. Samples were treated with or without RNase A. **d**, and **e**, Representative IF of RRBP1 (**d**), vigilin (**e**) co-stained with RNA fluorescent in situ hybridization targeting (RNA-FISH) of DENV or ZIKV positive stranded RNA genomes. Representative images of $n = 2$ biologically independent replicates showing similar results. Scale bars, 10 μm.

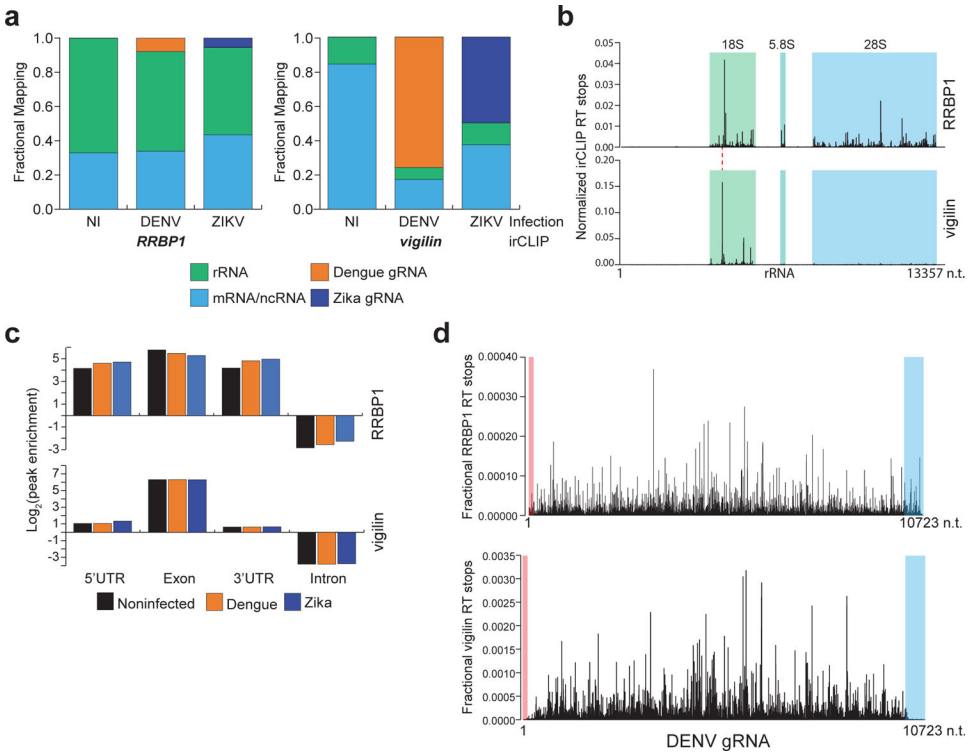

Fig. 4. DENV and ZIKV co-opt the RNA binding properties of RRBP1 and vigilin in human cells.

a, RRBP1 (left) and vigilin (right) irCLIP reverse transcriptase (RT) stop mapping statistics annotated to the human, DENV, or ZIKV genomes and the ribosomal RNAs (rRNA) from Huh7.5.1 cells infected with MOI of 0.1 for 48 h. **b**, Histogram of RT stops mapping to the rRNAs from the RRBP1 (top) and vigilin (bottom) irCLIP in uninfected Huh7.5.1 cells. The three cytosolic rRNAs are highlighted. Red dashed line denotes vigilin's strongest binding site, which is adjacent to RRBP1's. **c**, Annotation of peaks called from RRBP1 (top) and vigilin (bottom) irCLIP RT stops mapping to functional elements of human mRNAs including 5'UTR, exons, 3'UTR, and introns. Enrichment values are calculated based on the size of each function domain relative to the human genome. **d**, RRBP1 (top) and vigilin (bottom) irCLIP RT stops mapped at base resolution to the DENV genome. RT stop intensity was normalized to the total number of unique reads mapping to the viral genome. The 5'UTR and 3'UTR regions are highlighted in red and blue, respectively.

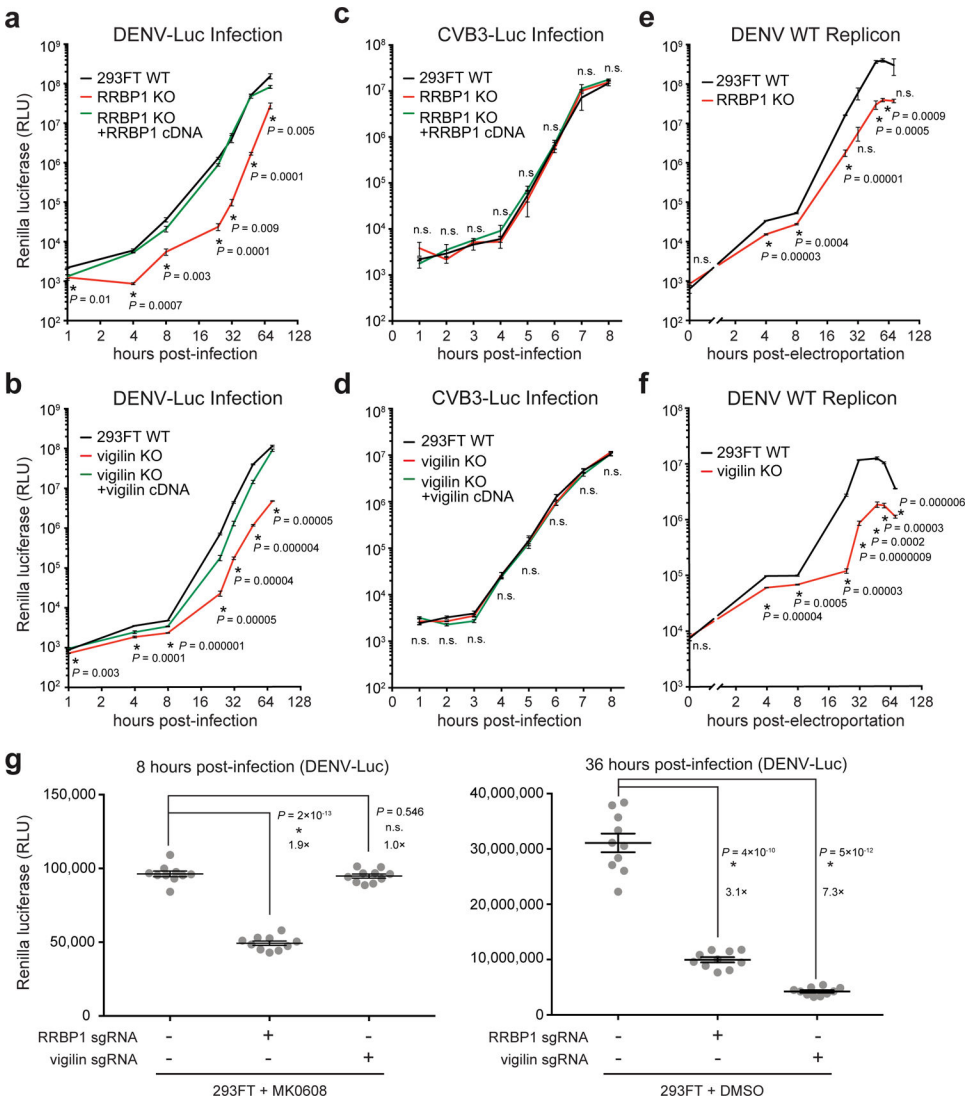

Fig. 5. RRBP1 and vigilin modulate DENV translation and replication.

a, and **b**, Time-course DENV-Luc infection assays. WT, RRBP1-KO, and RRBP1-KO + RRBP1 cDNA rescue (**a**) or WT, vigilin-KO, and vigilin-KO + vigilin cDNA rescue (**b**) HEK293FT cells were infected with DENV-Luc (MOI of 0.01) and harvested at indicated time points. Virus infectivity was then determined by measuring *Renilla* luciferase expression from infected cells. **c**, and **d**, Time-course CVB3-Luc infection assays. WT, RRBP1-KO, and RRBP1-KO + RRBP1 cDNA rescue (**c**) or WT, vigilin-KO, and vigilin-KO + vigilin cDNA rescue (**d**) HEK293FT cells were infected with CVB3-Luc (MOI of 1) and harvested at indicated time points. **e**, and **f**, Luciferase expression of luciferase-encoding DENV replicon RNA in WT and RRBP1-KO (**e**) or WT and vigilin-KO (**f**) HEK293FT cells over indicated time points post-electroporation of replicon RNA. The data in each panel (**a**-**f**) represent the mean with SEM of of $n = 3$ independent biological replicates. **g**, Luciferase expression 8 hours (left) post-DENV-Luc (MOI of 0.025) infection in the presence of the replication inhibitor MK0608 (50 μM final concentration) or 36 hours (right) post DENV-Luc infection in the presence of DMSO of WT, RRBP1-KO, and vigilin-KO HEK293FT

cells. The data in each panel represents the mean with SEM of 10 biologically independent infections. Fold change between datasets is indicated. All *P*-values stated in this figure were determined by two-tailed, unpaired *t*-test using GraphPad Prism, where * = $P < 0.05$ and n.s. = non-significant.

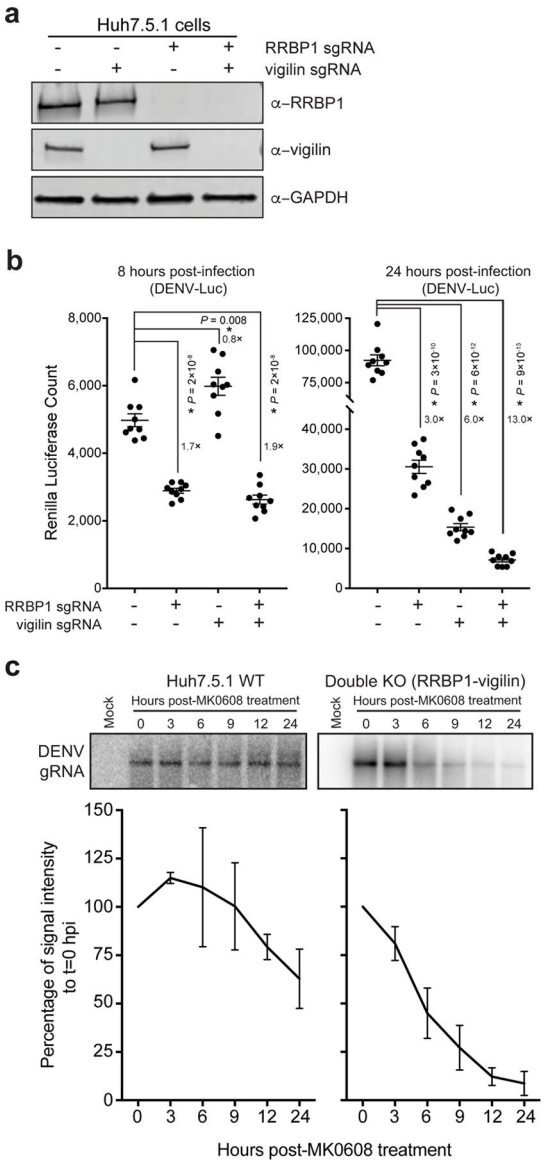

Fig. 6. RRBP1 and vigilin promote DENV infection and viral RNA stability.

a, Western blot analysis of WT Huh7.5.1, vigilin-KO, RRBP1-KO, and RRBP1-vigilin double-KO cells. Representative WB of $n = 2$ biologically independent replicates showing similar results. **b**, Luciferase expression at 8 hpi and 24 hpi upon DENV-Luc infection (MOI 0.01) of WT Huh7.5.1, vigilin-KO, RRBP1-KO, and RRBP1-vigilin double-KO cells. The data in each panel represent the mean and SEM of 9 biologically independent infections. The *P*-values were determined by two-tailed, unpaired *t*-test using GraphPad Prism, where * = $P < 0.05$ and n.s. = non-significant. **c**, Northern blot analysis of dengue genomic RNA extracted from WT Huh7.5.1 and RRBP1-vigilin double-KO cells that were first infected with DENV-2^{16681} (MOI of 0.1) for 48 hours, followed by MK0608 replication inhibitor treatment for indicated time frames (top panel). Quantification of DENV genomic RNA (i.e.

northern blot signal) from 3 independent experiments (error bars are SEM) as a percentage relative to time point 0 hour after MK0608 treatment (bottom).